in order to estimate the unsteady and non-uniform thermal environment formed close to the human body, these thermoregulation models consider multiple nodes divided along the human body, and each thermoregulation model uses particular models to evaluate the heat transfer phenomenon between skin surfaces and surrounding environments, heat transfer and exchange caused by blood flow, and heat loss by respiration. In the previous thermoregulation model, especially with the heat and moisture transfer phenomenon through respiration, macroscopic results for convective and evaporative heat transfer coefficients were adopted by assuming the simplified cylindrical tubes generally used in heat transfer engineering fields [23]. In addition, those results were adopted in order to calculate the heat transfer rate of the respiratory tract on the assumption of physical uniformity inside the airway. This means that the prediction method concerning respiratory heat loss was simpler and of lower accuracy than heat transfer/heat exchange modeling for other parts/nodes of the human body. Hence, in order to contribute to the improvement of prediction accuracy of the thermoregulation model for skin surface temperature, detailed analysis of the sensible and latent heat transfer phenomena inside the respiratory tract is considered as crucial and important.

Furthermore, the respiratory tract system is the portal between the human body and the indoor environment; hence, this is also the body's first line of defense against harmful pollutants from the surrounding indoor air. An investigation of airflow characteristics in the human respiratory tract provides valuable information to enhance the understanding of the transportation of inhaled particles and/or gas-phase contaminants through respiration [24,25].

Past experimental results show that the airflow has to pass through in the respiratory tract to reach 37 °C [26,27]. Airway temperature significantly increased within the nasal valve and turbinate part of the nasal airway. Measurements of the mean end-inspiratory temperature along the nasal cavity during inspiration at room temperature revealed values of 25.3 °C in the nasal vestibule, 29.8 °C in the nasal valve area, 32.3 °C in the anterior turbinate area (near to the head of the middle turbinate), and 33.9 °C in the nasopharynx [28]. The nasopharyngeal temperature was gained up to 34 °C according to results of different research papers [29,30]. The air temperature within the nasopharynx is close to the temperature of the nasal mucosa [31,32]. The contact time of inspired air with the mucosa lining of the anterior section of the nose providing sufficient warm the inspired air although the airflow has a high velocity in this part of the nose [33]. At the end of inspiration, the air temperature quickly increases during rest of breathing.

Experiments of temperature within the nasal cavity or human airway of the human are limited due to the complex anatomy and the very narrow nasal passageways. Furthermore, problems of temperature and humidity measurements are the tight spatial and limited time resolution. To fill this gap, CFD simulation was gradually applied to replace experimental work. Numerical simulation is utilized for manipulating and reflecting a real environment of complex geometries within a computational model. Technical improvement led to a large number of CFD studies within the last decade providing incremental knowledge research about the complex functions of human airways [34–36]. CFD simulations have performed to predict airflow pattern characteristics in combination with intranasal air temperature under various conditions [37–40]. CFD is considered a practical technique to reveal the relationship between intranasal airflow and heat transfer. Changes in temperature are strongly affected by airflow patterns. Numerical simulations applying CFD might provide a detailed information and visualization of airflow patterns within the entire respiratory tract even during a breathing cycle. Therefore airflow characteristics like turbulence characteristics, average air-velocity, volume flow, pressure conditions, distribution patterns and path lines should be investigated for varying inhalation airflow rates. Most of up to date studies simulated a steady inflow. CFD simulations of human airway temperature as functions of convective heat transfer and airflow during a steady and unsteady breathing condition have not been substantially discussed.

Against this background, this paper reports on the numerical prediction of airflow and temperature distribution in the human respiratory system as a function of the breathing airflow rate, targeting two types of numerical airway models (Model A and Model B). In addition, convective heat transfer phenomena in the airway

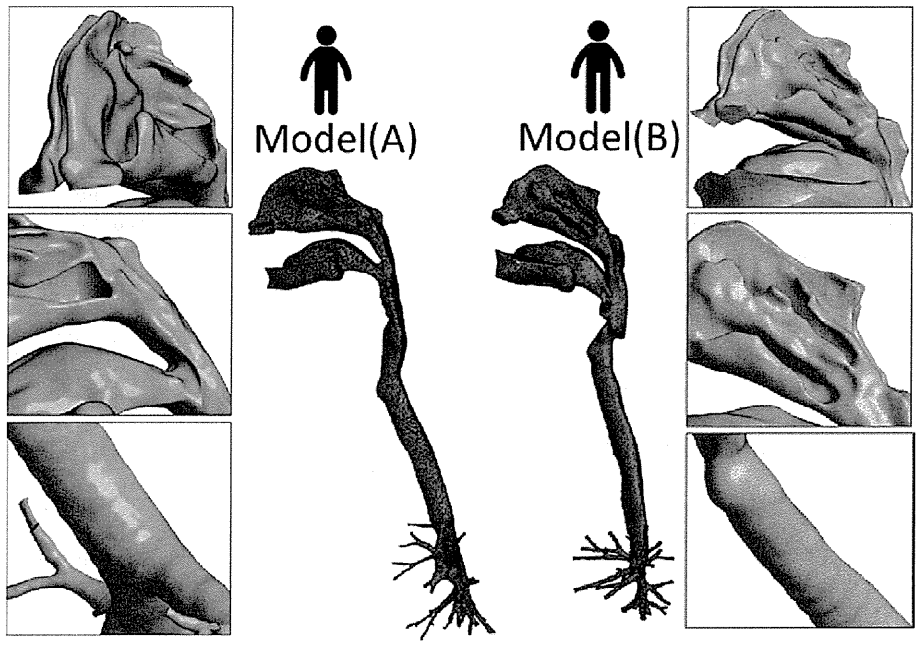

Fig. 1. Two types of numerical airway models (Model A and Model B).

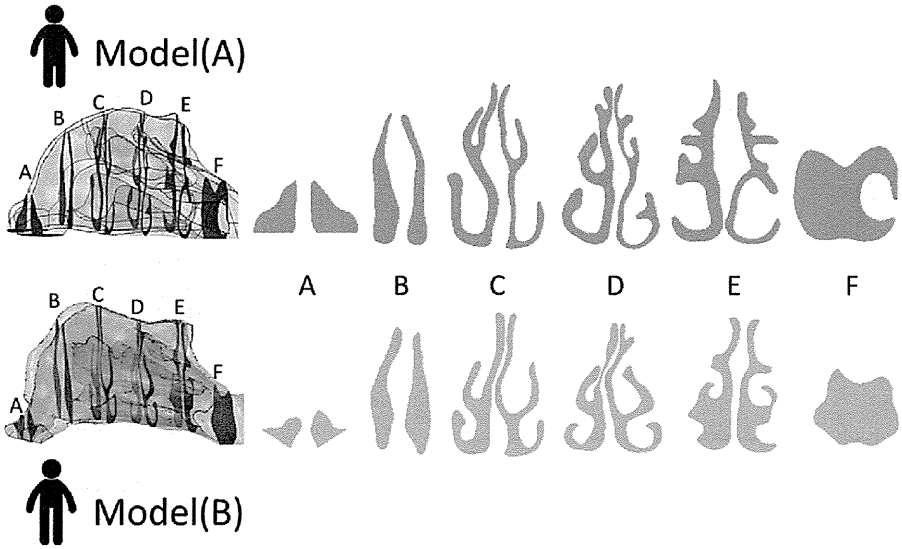

Fig. 2. Detailed geometrical differences of nasal cavities in Model A and Model B.

Table 1
Detailed geometrical information of two airway models.

	Model A	Model B
Height (m)	3.48×10^{-1}	2.74×10^{-1}
Nostril Area (m^2, right side opening)	1.29×10^{-4}	0.80×10^{-4}
Surface Area (m^2)	5.99×10^{-2}	4.46×10^{-2}
Volume (m^3)	1.73×10^{-4}	1.29×10^{-4}
Equivalent diameter at trachea (cross-section, m)	1.669×10^{-2}	1.650×10^{-2}
Loading Factor (m) (=Volume/Surface)	2.89×10^{-3}	2.88×10^{-3}

Table 2
Numerical and boundary conditions of CFD.

Turbulence Model	Low-Reynolds-number-type k-ε model (Abe–Kondoh–Nagano model)
Mesh	7.5 million unstructured mesh (Model A) 4.1 million unstructured mesh (Model B) (y^+ <1 for the first grid point)
Scheme	Convection term: second-order upwind
Inflow Boundary	Q_{in} = 5, 7.5, 15, 30, 60 L/min, (steady inhalation) $k_{in} = 3/2\ (U_{in} \times 0.05)^2$, $\varepsilon_{in} = C_\mu^{3/4} k_{in}^{3/2} / l_{in}$, T_{air} = 20 °C (=293 K)
Outflow Boundary	U_{out} = free slip, k_{out}, ε_{out} = free slip
Wall Treatment	Velocity: no slip Temperature: $T_{wall\ surface}$ = 36.8 °C (=309.8 K)

Table 3
Inhalation average velocities at nostril surfaces and average velocities at trachea corresponding to air flow rates.

Air flow rate (Average breathing rate)	Model A	Model B
5 L/min	0.32 m/s at nostril 0.38 m/s (*Re* = 435) at trachea	0.52 m/s at nostril 0.39 m/s (*Re* = 440) at trachea
7.5 L/min	0.48 m/s at nostril 0.57 m/s (*Re* = 652) at trachea	0.78 m/s at nostril 0.58 m/s (*Re* = 660) at trachea
15 L/min	0.96 m/s at nostril 1.14 m/s (*Re* = 1306) at trachea	1.56 m/s at nostril 1.17 m/s (*Re* = 1320) at trachea
30 L/min	1.92 m/s at nostril 2.29 m/s (*Re* = 2612) at trachea	3.12 m/s at nostril 2.34 m/s (*Re* = 2642) at trachea
60 L/min	3.84 m/s at nostril 4.57 m/s (*Re* = 5224) at trachea	6.24 m/s at nostril 4.68 m/s (*Re* = 5284) at trachea

(Upper stage: average velocity at nostril surface [m/s], (Lower stage: average velocity at trachea [m/s] and *Re* number calculated by average velocity at trachea and equivalent diameter of trachea cross-section).

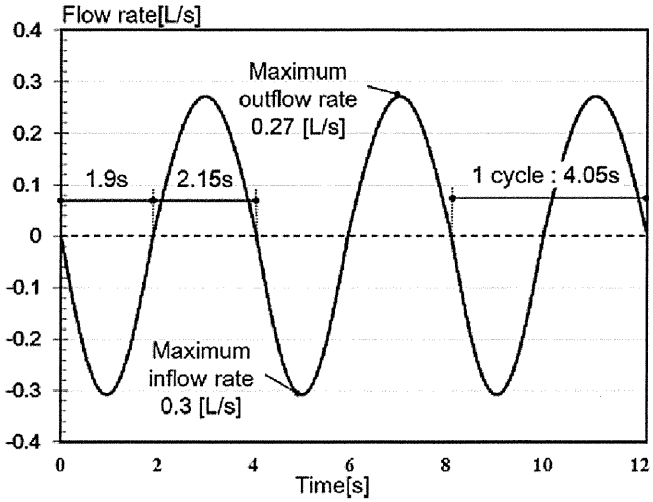

Fig. 3. An unsteady breathing cycle.

models are discussed by estimating the convective heat flux and convective heat transfer coefficients (CHTCs) of each human airway segment under various breathing conditions using CFD. The database of CHTCs in the human respiratory system as a function of breathing air flow rate will contribute to the development and improvement of the convective heat transfer models in thermoregulation models.

On the other hand, physiologically based pharmacokinetic (PBPK) models which harmonized computational fluid dynamics simulation in numerical respiratory tract model have been discussed and developed [41–44]. PBPK model is expected to estimate comprehensive risk of inhalation exposure in indoor environments and for decades, pharmacokinetic models have been successfully applied to address issues of extrapolation between contaminants, dose, dose-rate/dose–response, or types of exposure to drugs or chemicals. Generally, partition coefficient concept between air and tissue boundary and mass transfer coefficient of target contaminant will be adopted in simplified PBPK model. Assuming an analogy between heat and mass transfer in the airway model, the relationship between convective heat transfer coefficient and mass transfer coefficient can be expressed through the Lewis number (*Le*) concept. The Lewis number of gaseous matter is known to be approximately constant, meaning that CHTCs represents mass transfer efficiency and CHTCs can give a good approximation of mass transfer coefficient for vapor and volatile organic compounds [45]. In this point of view, CHTCs database makes it possible to apply hygrothermal transfer and inhalation exposure analysis in human respiratory tract.

2. Materials and methods

In this study, numerical airway models were created by using original computed tomography (CT) data, and CFD analysis of flow and temperature distributions inside numerical airway models were conducted.

2.1. Computational model generation

We developed two types of numerical airway models. Original respiratory tract data were obtained using a Toshiba 64 multi-detector-row computed tomography (MDCT) scanner. The subjects included a nonsmoking, healthy Asian male for Model A and a nonsmoking, European male of almost the same age and height for Model B. As for Model A, geometrical details have been reported in our previous paper [8].

CT scans produce images of continuous slices of the respiratory tract and store them as standard digital imaging and communications in medicine (DICOM) data, a format commonly used for the transfer and storage of medical images. A set of 785 cross sections (slices) were obtained and the original set of CT images was converted into a file format compatible with Mimics® (Materialise NV), which is 3D imaging software that generates and modifies 3D surface models from medical images. Generation of a surface model from 2D contour data began with the translation of the segmented, modified, and smoothed contour points into a data series that was loaded into the ANSYS preprocessing software packages TGrid and ICEM [46]. These mesh generation programs were used to modify the surface mesh and to create a volume mesh of the model, respectively. The first mesh wall surface is set within the viscous sub-layer and the wall units (y^+), which express the dimensionless normal distance from the surface, satisfying the requirement of 1.0 or less over the whole surface of each airway model. The mesh resolution of CFD simulation in this study is on the order of 0.01–0.1 mm (10–100 μm). The adequacy of grid resolution was tested by verifying fluid result at the flow rate of 7.5 L/min and carefully compared with the experimental data. For example, four levels of grid resolution were adopted: 1.0 million, 4.6 million, 7.5 million, and 10.6 million total meshes in Model A and the human airway geometry in case of 7.5 million meshes was confirmed to be sufficient for predicting accuracy in this study. In this CFD simulation, grid independence check was carefully and elaborately executed and minimum mesh size in the vicinity of wall surface, skewness and size ratio of adjoining mesh were elaborately designed [9–12,47]. Details of mesh independence test and comparison with PIV (particle image velocimetry) experimental results were discussed in our previous paper [8].

Fig. 1 shows external views of two types of numerical airway models (Model A and Model B) and Fig. 2 denotes the detailed geometrical differences of nasal cavities in the two models (Model A and Model B). Table 1 also summarizes detailed size information for the two airway models (Model A and Model B).

2.2. Outline of CFD simulation

CFD simulations were performed to calculate airflow, temperature, and heat transfer profiles under five types of breathing conditions. Steady and transient flow fields were analyzed using a low-Reynolds-number (low-Re) k-ε model (the Abe–Kondoh–Nagano model) [48,49]. This low-Re k-ε model (Abe–Kondoh–Nagano model) has been adopted for the various types of flow field analysis (from laminar to turbulence) and confirmed the good prediction accuracy to flow and thermal field analysis intended the near-wall and low-Reynolds-number effects in both attached and detached flows [8]. A no-slip boundary condition was applied for the wall surfaces inside the airway model. The second-order upwind was used for the convection term, and a SIMPLE (semi-implicit method for pressure-link equations) algorithm was used [50]. The value of turbulent kinetic energy at the inlet, i.e., at the nostril, was prescribed assuming a 10% turbulence intensity. The turbulence intensity was set corresponding to experimental study of Stapleton et al. [51].

In this study, airflow rates of 5.0, 7.5, 15, 30, and 60 L/min, i.e., the transition from the laminar to the turbulent flow regime, were considered. In addition to the air supply function of the human nasal cavity, heat and mass transfer conditions for regulating heat release from the core of the human body through the respiratory tract are also important. Here, the air conditioning capabilities of the airway model in terms of its heat transfer were simulated for

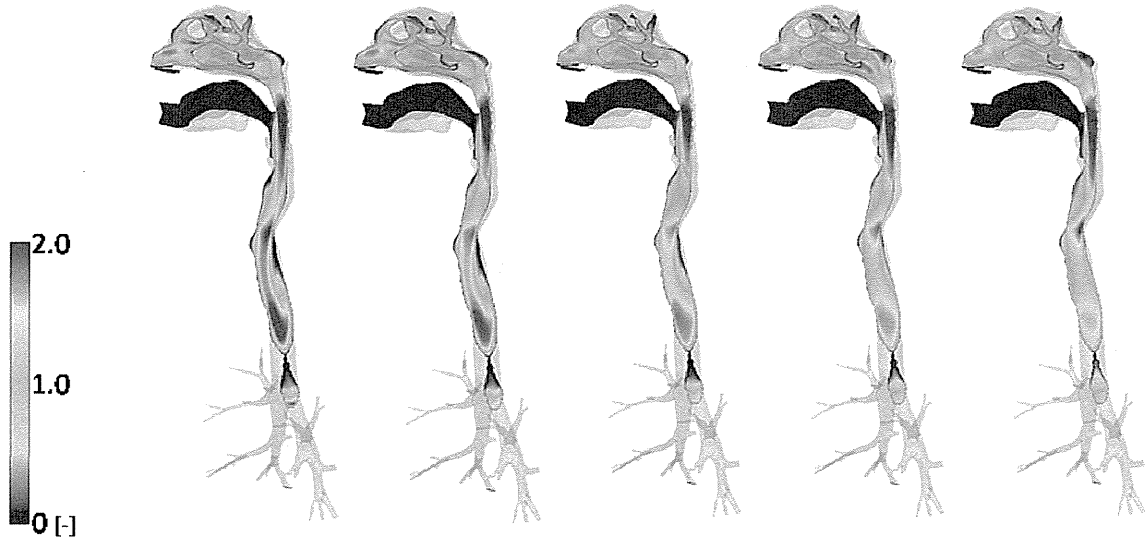

Q_{air} [L/min]	5	7.5	15	30	60
Reynolds Number	292	437	874	1747	3494

(1) Model A

Q_{air} [L/min]	5	7.5	15	30	60
Reynolds Number	474	710	1420	2840	5678

(2) Model B

Fig. 4. Normalized scalar velocity distributions in airway models.

different flow rates. Room air at a temperature of 20 °C was used in the simulation as the inhaled ambient air, and the inner walls, which are covered by a layer of mucus tissue, were assumed to be at a constant temperature of 36.8 °C. The numerical and boundary conditions are summarized in Table 2. Table 3 shows the cases analyzed as a function of the flow rate of inhaled air, assuming steady state.

Furthermore, in order to discuss the validity of steady-state analysis, adopting steady respiratory airflow rate as shown in Table 3, an unsteady breathing cycle was reproduced and was considered as a transient inhalation/exhalation boundary condition of the airway model. In this study, the unsteady respiratory cycle model proposed by Gupta et al. and revised by Kadota et al. was used as the basic breathing airflow model [52–54]. This transient breathing model is the source model for determining thermo-fluid conditions of the air inhaled/exhaled during breathing, and we assume this breathing model in setting the boundary conditions at the nostril surfaces. The transient breathing airflow rates in this

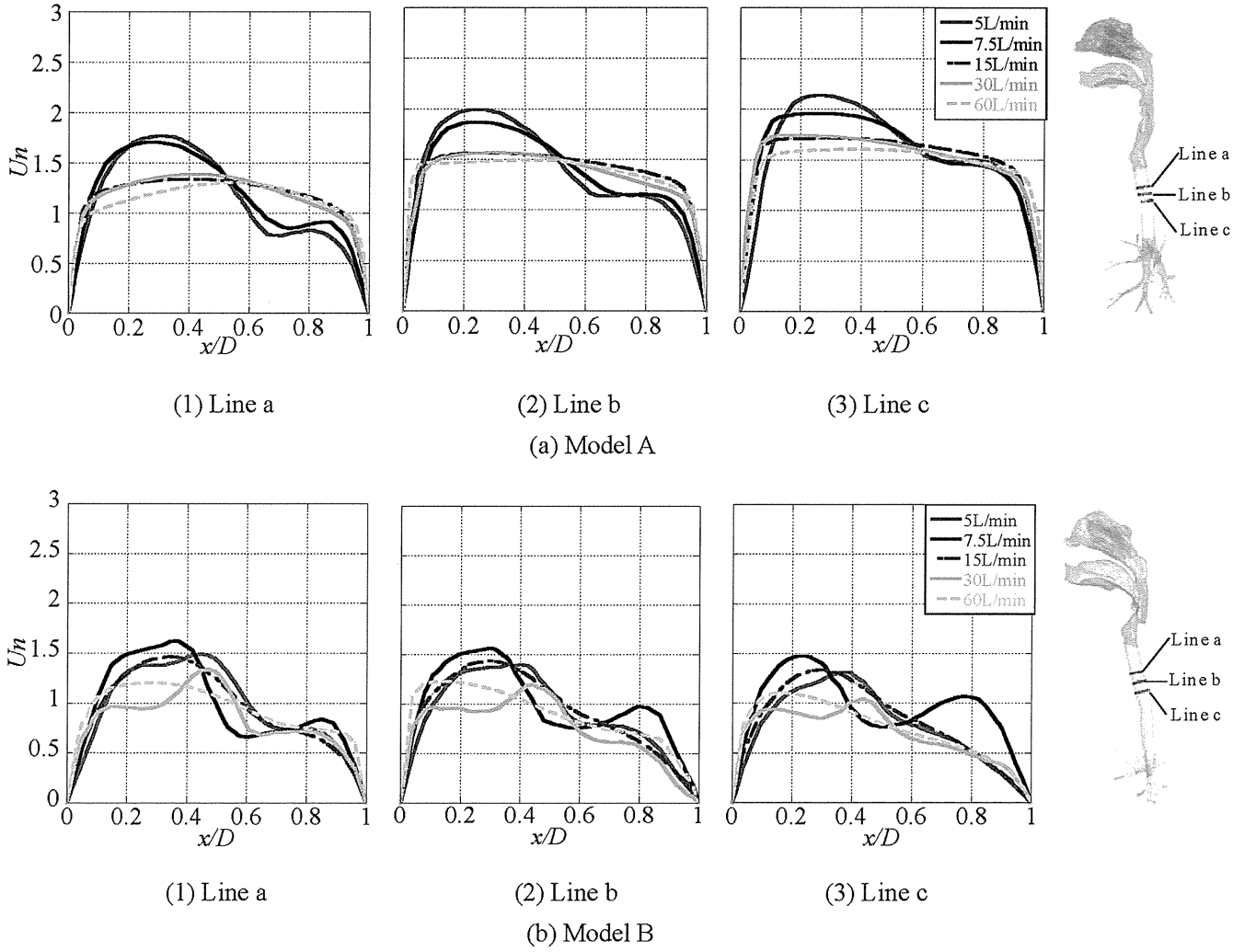

Fig. 5. Comparison of non-dimensional scalar velocity distributions in airway models.

study are shown in Fig. 3.

2.3. Convective heat transfer coefficient

The respiratory convective heat transfer coefficient (CHTC) is a phenomenological constant relating the heat flux to the temperature difference between the free airstream and airway walls (the lumen or airway tissue surface, in this research). The widely accepted expression for the CHTC (h_c) is as follows:

$$h_c = \frac{Q_c}{(T_w - T_{air})} \quad (1)$$

Here, Q_c implies that the convective heat flux [W/m^2] T_w is the constant tissue wall surface temperature [K], and T_{air} is the air inhaled (ambient) in the airway model [K].

3. Results and discussion

In a previously reported paper [8], a realistic replica model which made using a transparent acrylic material was created and the particle image velocimetry (PIV) technique was applied to measure flow patterns in the human upper airway model. The prediction accuracy of CFD analysis in the present human airway model (Model A) was validated with experimental data sets from laminar to turbulent flows under isothermal conditions. CFD simulation results using a low-Reynolds-number k–ε model agreed reasonably well with results measured by PIV. The results of CFD analysis concerning flow, temperature, and convective heat flux distributions are shown in this section and discussed along with the averaged CHTCs and their distributions.

3.1. Airflow and temperature fields

Some selected results from numerical simulations for different inspiratory flow rates are given in the following section. The corresponding Reynolds number (*Re* number) in the trachea for all cases analyzed are also listed in Table 3.

3.1.1. Airflow field

Fig. 4 shows contours of the normalized velocity magnitude ($U_n = U/U_{in}$) in the vertical plane (y–z plane) for inspiratory flow rates from 5 to 60 L/min in Model A and Model B. The airflow in the nasal cavity for both cases showed complicated flow patterns and separation posterior to the narrowest valve and acceleration through the middle region of the nasal cavity because of the reduction in cross-sectional area. At the pharynx, accelerated air flow was observed in the curved geometry from the nasal cavity to the pharynx/larynx. A clear difference in the flow patterns in the

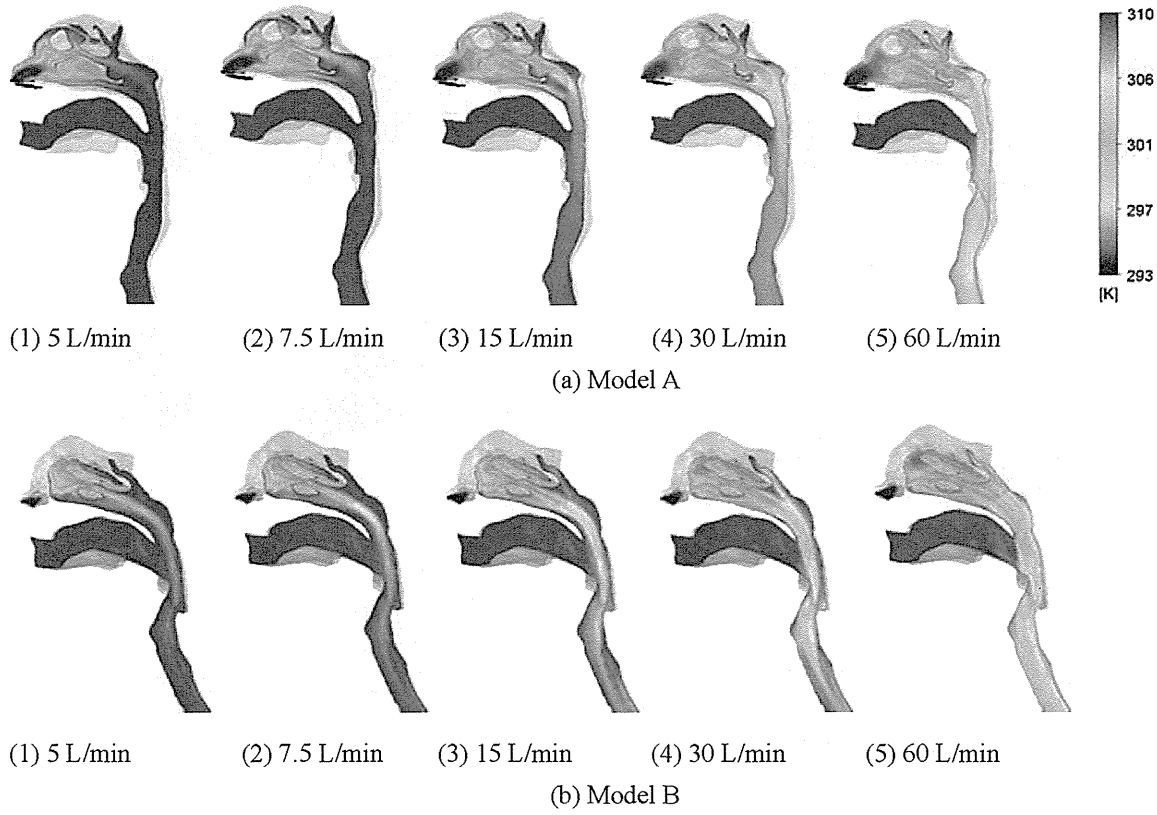

Fig. 6. Temperature distributions in airway models.

laryngeal flow, which forms immediately after the glottis region, was observed in Model A and Model B.

Comparing the flow pattern at 5 L/min and 60 L/min cases in Model A, clear differences in the tracheal region were confirmed, representing the Reynolds number dependence of flow fields in the airway models.

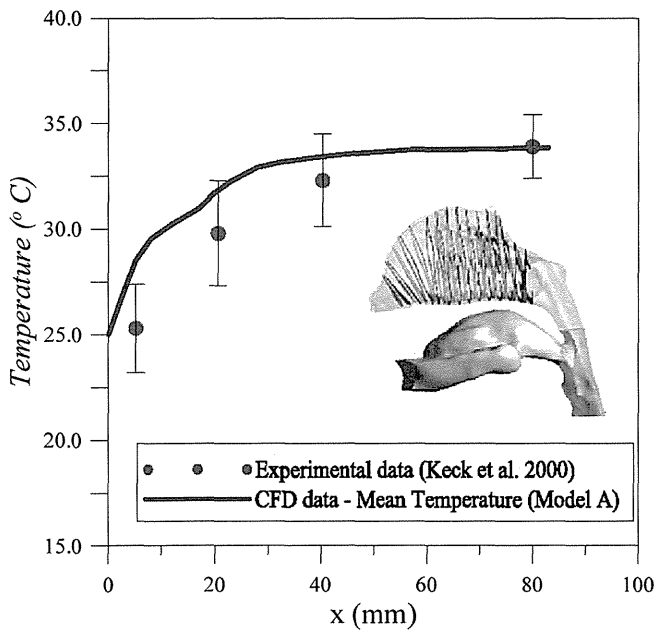

Fig. 7. Temperature profiles across the nasal cavity in the case of model A.

Fig. 5 shows the comparison of non-dimensional scalar velocity distributions in the tracheal region for two airway models (Model A and Model B). In Model A, obvious non-uniform flow patterns were observed in the cases of 5, 7.5, and 15 L/min flows, but relatively uniform flow patterns were formed in the cases of 30 and 60 L/min flows. Air was mixed well at higher respiratory airflow rates; in these cases, the flow pattern in the tracheal region became uniform.

On the other hand, in Model B, the trend was for air velocity distribution to become relatively smoother and more uniform with increasing respiratory airflow rate, but flow patterns in the tracheal region of Model B were complicated compared to those of Model A.

3.1.2. *Temperature distribution*

Fig. 6 shows the temperature distributions in the human upper airways of Model A and Model B. For example, at flow rates of 5, 7.5, and 15 L/min in Model A, a relatively low temperature was observed at the vestibule, and the air temperature in the lower airway region became well-mixed. Thus, the temperature distribution tended to be uniform from the pharynx to larynx. Moreover, the air temperature from the nostrils was affected more rapidly at low airflow rates of 5.0, 7.5, and 15 L/min compared to results at 60 L/min because the low flow rate induces a longer residence time for air in the airways.

In Model B, the same discrepancies in temperature distributions were confirmed compared with those in Model A. In particular, respiratory air of relatively lower temperature was transported directly from the nasal cavity to the pharynx and tracheal region in Model B. These differences were ascribed to individual differences between different respiratory tracts.

Temperature distributions and prediction accuracy of our airway model were validated with *in vivo* experimental data from literature. As for the temperature distributions in the upper

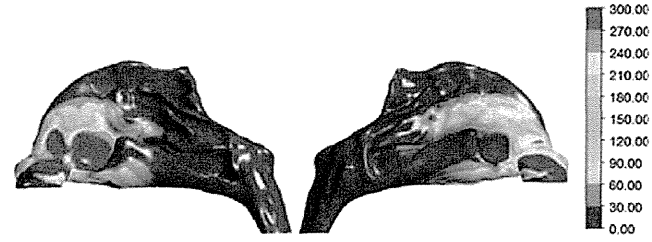

(1) 5 L/min

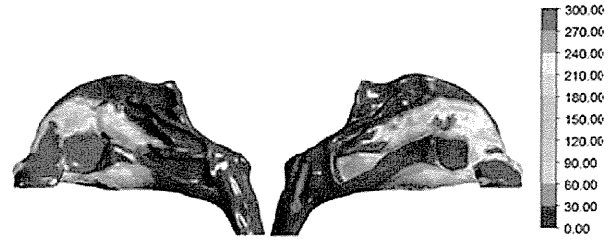

(2) 7.5 L/min

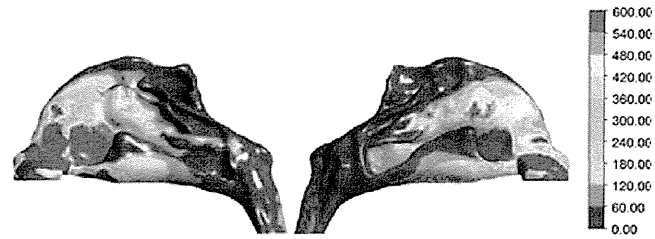

(3) 15 L/min

(4) 30 L/min

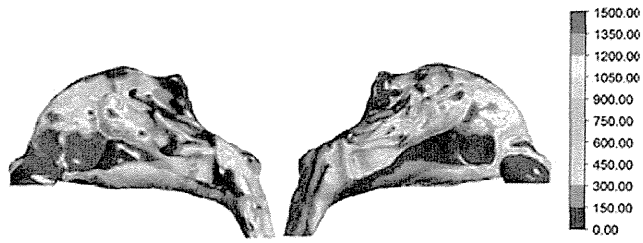

(5) 60 L/min

(a) Model A

Fig. 8. Convective heat flux distributions on the upper airway surfaces [W/m^2].

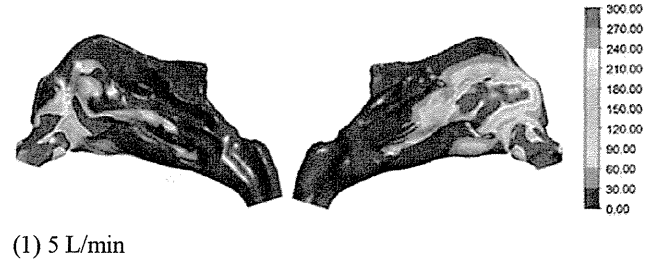

(1) 5 L/min

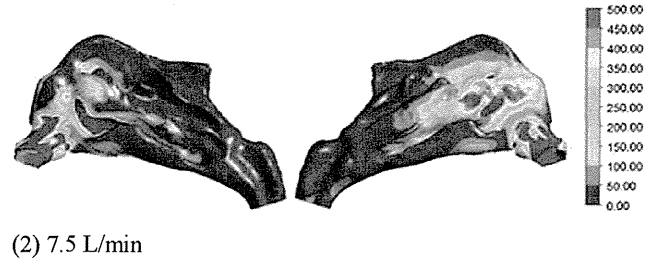

(2) 7.5 L/min

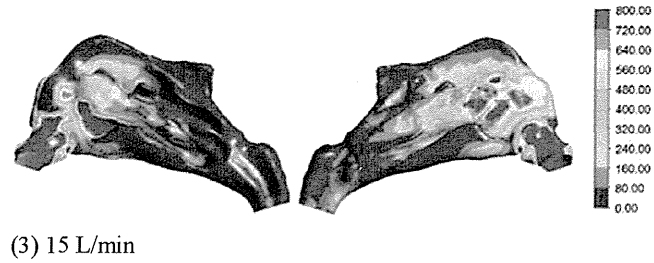

(3) 15 L/min

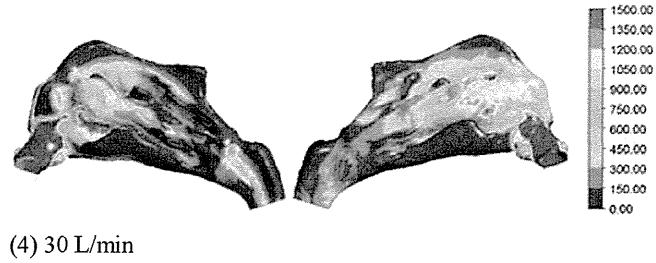

(4) 30 L/min

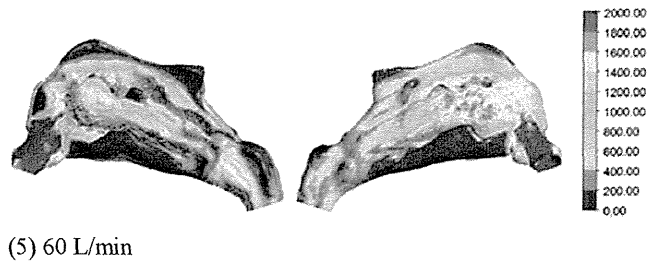

(5) 60 L/min

(b) Model B

Fig. 8. *continued.*

respiratory tract, Keck et al. reported *in vivo* measurements [28,55] at several distances from the nostrils, forming a range of experimental data. In this measurement, 4 temperature points from the external nostrils to the pharynx were measured precisely to target a total of 23 subjects at under 25 °C and 35%RH ambient air conditions. In order to discuss the prediction accuracy of non-isothermal CFD analysis, we conducted additional CFD simulations at 25 °C ambient air temperature conditions corresponding to the experimental conditions reported by Keck et al. Temperature profiles were obtained from the average temperature at each cross-section throughout the airway for a breathing rate of 7.5 L/min, so that comparisons could be made with experimental work. The temperature distributions from CFD and *in vivo* measurements are shown in Fig. 7. The profile showed a discrepancy in the frontal regions towards the turbinate section and gradually becoming good agreement in the distal regions of the nasal cavity. The profile converged to a steady value at a distance of 80 mm from the inlet.

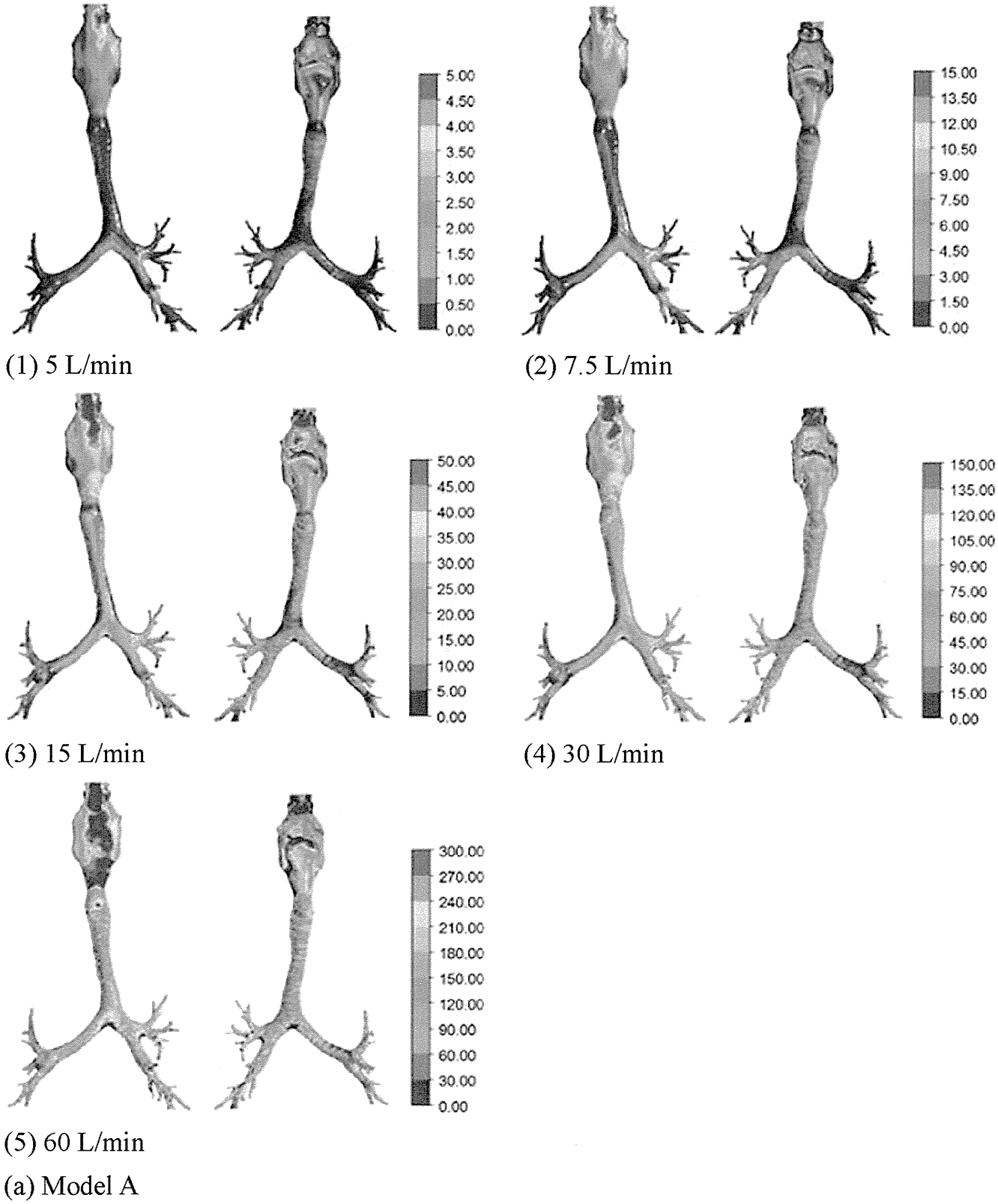

Fig. 9. Convective heat flux distributions on the lower airway surfaces [W/m^2].

These were reasonably consistent with each other, and the deviations between predictions and measurements were close to the measurement accuracy (i.e., ±1.5 °C to ±2.5 °C).

3.2. Heat flux and convective heat transfer coefficient

In this analysis, we adopted a low-Re k-ε model to resolve the

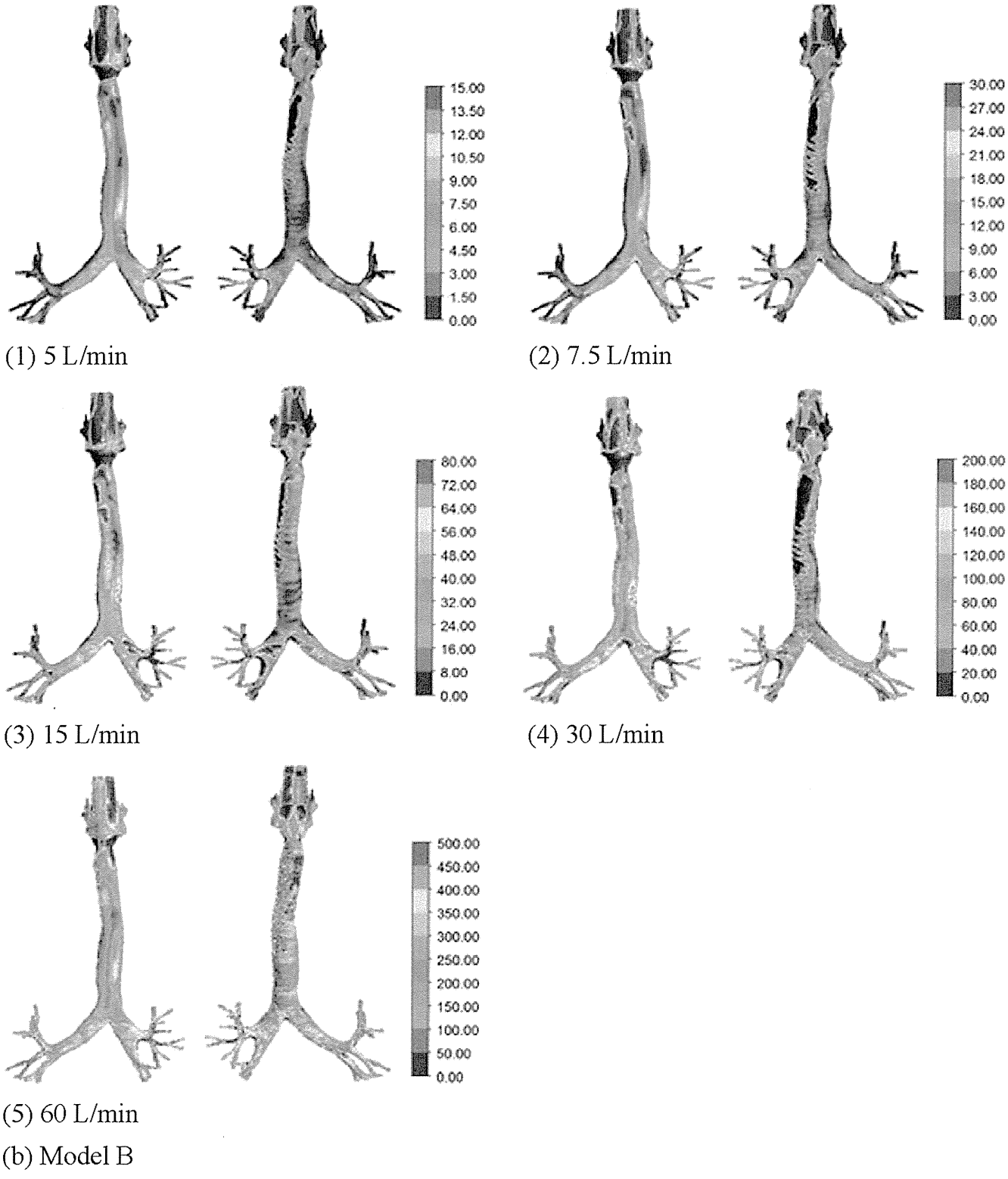

Fig. 9. *continued.*

detailed flow profile inside the viscous sub-layer and thermal boundary layer on tissue surfaces. Subsequently, convective heat flux was analyzed precisely.

The wall heat flux distributions in the upper and lower airway regions are shown in Figs. 8 and 9, respectively. In both cases (Model A and Model B), the highest heat flux regions were observed at the nostrils because of the large temperature difference between ambient air and the tissue wall surfaces. Relatively high heat flux regions expanded with increasing respiratory airflow rate. As for the lower airway regions, the relatively high wall heat flux appeared at posterior regions of the oral-pharynx where temperature gradients increased. The lower sections of the airway

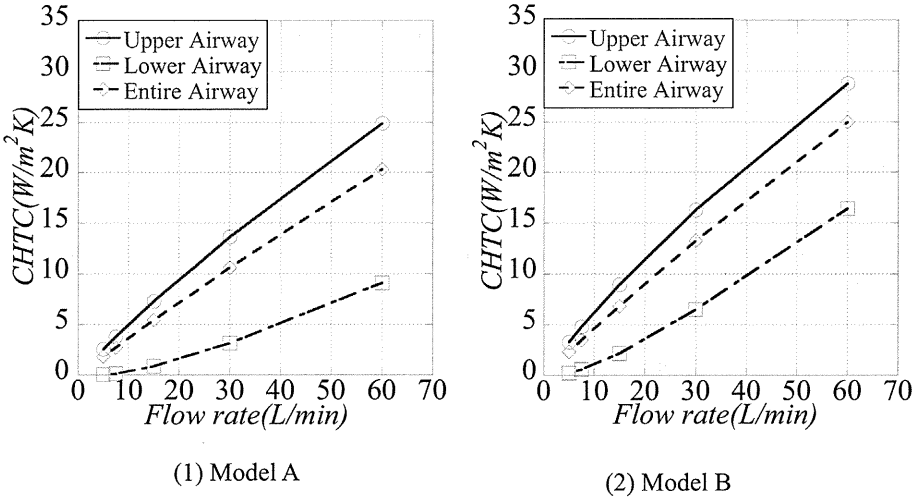

Fig. 10. Convective heat transfer coefficient (CHTC) as a function of breathing airflow rate.

Table 4
Average convective heat transfer coefficient (CHTC) for each breathing air flow rate condition [W/m²K].

		5 L/min	7.5 L/min	15 L/min	30 L/min	60 L/min
Model A	Upper Airway	2.542	3.766	7.271	13.64	24.89
	Lower Airway	0.02911	0.1240	0.8484	3.150	9.093
	Entire Airway	1.815	2.712	5.412	10.61	20.32
Model B	Upper Airway	3.268	4.765	8.933	16.30	28.78
	Lower Airway	0.2159	0.5527	2.131	6.462	16.41
	Entire Airway	2.324	3.462	6.823	13.25	24.95

exhibited low fluxes because the flow of the inhaled air and temperature gradient decreased in those regions. In the region of the trachea and at bifurcations, a low heat flux value was confirmed in the case of low airflow rates, e.g., 5, 7.5, and 15 L/min, because the inhaled air adjacent to the walls had a temperature equal to the core body temperature. At 60 L/min, the values of the heat flux were still high even at the trachea and bronchial branches.

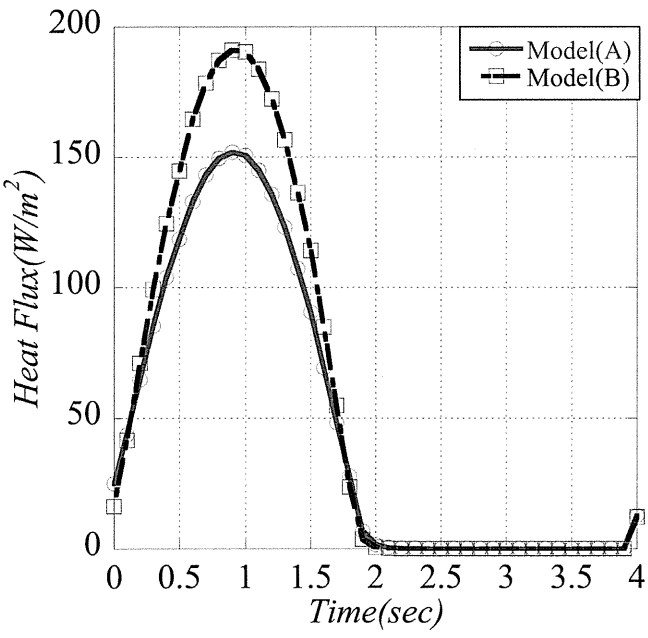

Fig. 11. Time series of heat flux on airway surfaces.

Fig. 10 and Table 4 show the area-weighted average convective heat transfer coefficient (CHTC) as a function of breathing airflow rate in Model A and Model B. With all analytical cases, a nearly linear relation between airflow rate and CHTC was confirmed. Although the tendency of the CHTC changes with respiratory airflow rate were almost the same for both Model A and Model B, approximately 20% differences of ĊHTC in Model A and Model B were confirmed. This result implies that the influence of individual specificity on convective heat transfer efficiency in the respiratory tract cannot be disregarded.

3.3. Convective heat transfer coefficient under a transient breathing cycle

Fig. 11 shows the time series of heat flux on airway tissue surfaces during one breathing cycle. Time-averaged airflow rate in the transient breathing cycle condition corresponded to 7.5 L/min. During the exhalation mode from $t = 0$ to $t = 1.9$ s, the convective heat flux from tissue wall surfaces in airway models was zero and the heat flux changed with the alternation of respiratory airflow rate during the inhalation mode from $t = 1.9$ to $t = 4.05$ s. Time-averaged CHTCs for Model A and Model B are summarized in Table 5. Time-averaged CHTCs for the transient simulation were reasonably consistent with those in the steady-state analysis under the $Q_{in} = 7.5$ L/min condition.

According an expression proposed by Fanger [56], sensible heat loss by respiration is normally calculated using the following simplified Equation (4):

$$C_{res} = 0.0014M(34 - T_a) \quad (2)$$

Equation (2) was basically derived from the assumption of simple circular cylinder geometry of the respiratory tract and hence a certain level of uncertainty was inevitable. Here, C_{res} indicates the rates of convective heat loss from respiration per unit area of body surface [W/m²], M indicates the rate of metabolic heat production [W/m²] and T_a represents ambient air temperature [°C].

If we assume the metabolic heat production rate M from 47.9 [W/m²] (=0.82 Met) to 75.5 [W/m²] (=1.3 Met), the rates of convective heat loss from respiration C_{res} becomes the range of 0.94 from 1.48 [W/m²]. Here if the body surface area (BSA) assumes to be the range of 1.6 [m²] from 1.8 [m²], convective heat

Table 5
CHTC, convective heat flux and total heat loss through airway for steady and transient breathing conditions.

	Model (A)	Model (B)
Steady (Q_{in} = 7.5 L/min)	2.712 [W/m^{2}K]	3.462 [W/m^{2}K]
	45.56 [W/m^2]	58.16 [W/m^2]
	2.729 [W]	2.594 [W]
Transient (Inhalation mode from t = 0–1.9 s in Fig. 10)	2.814 [W/m^{2}K]	3.416 [W/m^{2}K]
	47.28 [W/m^2]	57.39 [W/m^2]
	2.832 [W]	2.560 [W]

(Unit of [W/m^{2}K], [W/m^2] and [W] represent CHTC, convective heat flux per unit surface area of airway model, and total heat loss through airway model, respectively).

loss through respiratory system ($C_{res} \times BSA$) becomes the range of 1.50 from 2.66 [W]. The orders of these values are reasonably consistent with the simulation results of numerical airway models shown in Table 5.

3.4. Discussion

Nuckols et al. [57] reported detailed results of convective heat transfer experiments with a cast replica of human upper airways extending from the nose and mouth to the trachea. Considering inspiration only, Nuckols et al. expressed the experimental results in terms of *Nu* numbers averaged over the entire cast from the nose to trachea as follows:

$$Nu = 0.028(\mathrm{RePr})^{0.854} \tag{3}$$

The left-hand term in Equation (3) is the Nusselt number (*Nu*), which is commonly used as a dimensionless representation of the convective heat transfer coefficient for a given characteristic dimension. The term on the right-hand side of Equation (3) is a function of the Reynolds number (*Re*) and the Prandtl number (*Pr*), which are defined as the ratio between inertial and viscous forces in a fluid and the ratio of the molecular momentum diffusivity to the thermal diffusivity, respectively.

Definitions of *Nu*, *Re*, and *Pr* are as follows:

$$Nu = \frac{h_c D_T}{\lambda} \tag{4}$$

$$\mathrm{Re} = \frac{uD_T}{\nu} \tag{5}$$

$$\mathrm{Pr} = \frac{\nu}{\alpha} \tag{6}$$

where λ is the thermal conductivity of air (W/m/K), D_T is the diameter of the trachea (m), u is the representative axial velocity, ν is kinetic molecular viscosity, and α is the thermal diffusion coefficient.

Fig. 12 shows the regional convective heat transfer coefficient (CHTC) versus respiratory airflow rate, including the results shown in Fig. 9 and simulation results using Equation (3). In order to calculate *Nu* in Equation (4), the radius $r = 9.0 \times 10^{-3}$ m (=9 mm) and pipe length $l_p = 90.0 \times 10^{-3}$ m (=90 mm) (from nostril to pharynx in the upper airway) were adopted. Compared with the *in vitro* data obtained by Nuckols et al. [57] and the data assuming human airway model, a certain amount of discrepancies were observed. One of the reasons for these differences may be experimental uncertainty and inaccurate geometry in the human airway models used in this study compared with those in Nuckols et al. However, these differences were not extremely larger than differences between individuals (differences between Model A and

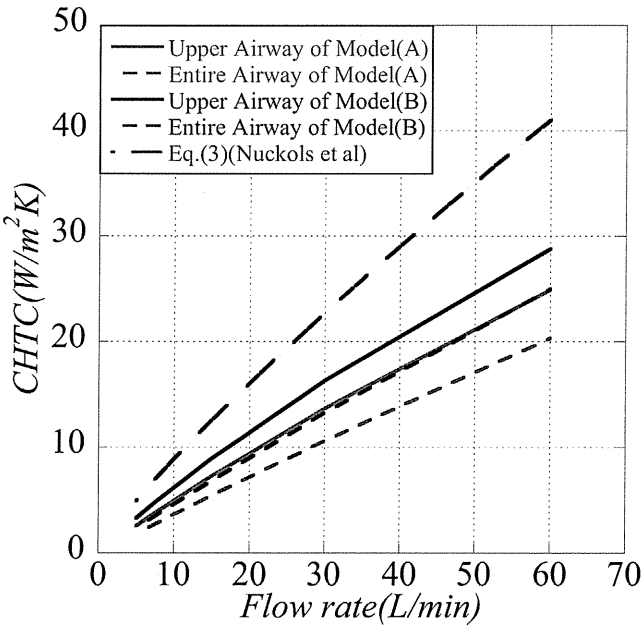

Fig. 12. Regional convective heat transfer coefficient (CHTC) versus respiratory airflow rate.

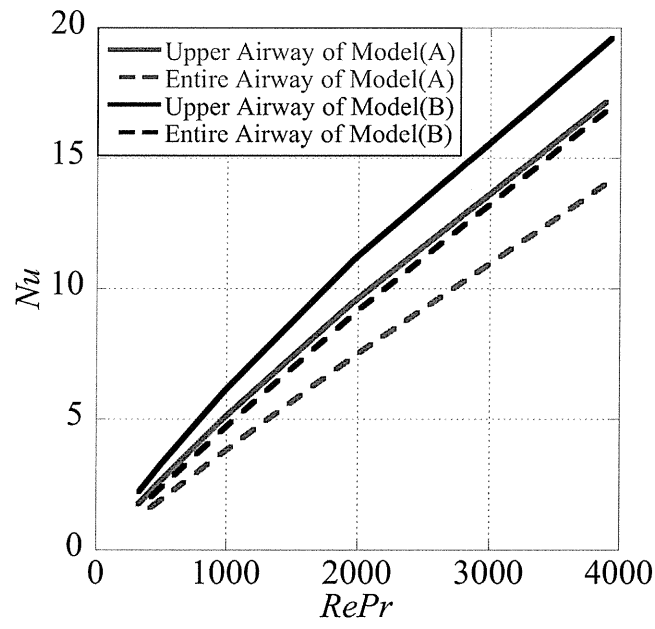

Fig. 13. *Nu* versus product of *Re* and *Pr* for upper and entire airways.

Table 6
Correlation of *Nu* versus product of *Re* and *Pr*.

Target airway model	Correlation function	Range of *Re*	Correlation coefficient
Human model A (Upper)	$Nu = 0.0088(\mathrm{Re}\cdot\mathrm{Pr})^{0.9192}$	$330 < \mathrm{Re} < 5300$	$r^2 > 0.99$
Human model A (Entire)	$Nu = 0.0045(\mathrm{Re}\cdot\mathrm{Pr})^{0.9741}$		
Human model B (Upper)	$Nu = 0.0142(\mathrm{Re}\cdot\mathrm{Pr})^{0.8768}$		
Human model B (Entire)	$Nu = 0.0063(\mathrm{Re}\cdot\mathrm{Pr})^{0.9573}$		

Model B). Generally, the respiratory tract is of complicated geometry and consists of elaborate parts; hence, it is difficult to accurately predict convective heat transfer phenomena.

The relationship between the Nusselt (*Nu*) number and the product of the Reynolds (*Re*) and Prandtl (*Pr*) numbers for the upper and entire airways is depicted in Fig. 13. Based on the numerical simulation results, the correlations between Nusselt (*Nu*) number and the product of the Reynolds (*Re*) and Prandtl (*Pr*) numbers are summarized in Table 6.

Correlation function of *Nu* versus product of *Re* and *Pr* for targeting upper airway region of Model B was reasonably consistent with the result (Equation (3)) reported by Nuckols et al. [57]. The results in Fig. 13 and Table 6 implied that the influence of the individual specificity, e.g. geometrical differences and size of respiratory tract, could be confirmed in the relation of *Nu* versus product of *Re* and *Pr*.

In this study, static geometries of human respiratory tract models, i.e. motionless and disregarding the expansion and contraction of airway geometries, were adopted because the main objective of this numerical analysis was to discuss the CHTCs in numerical airway models under steady state breathing conditions. However, when human breathes, the surface of human airway will have a possibility to stretch and shrink, which also influences the CHTCs. These are the potential limitation of this study. Recently, the progressive study about the effect of unsteadiness on the mixed convection boundary layer flow over a stretching and/or shrinking surface [58,59]. The discussion of these modeling and application will be the future challenge.

4. Conclusions

In this research, CFD with a low-Reynolds-number-type k-ε model was adopted for analyzing airflow and temperature distributions in numerical airway models. CFD analyses were carried out focusing on a wide range of airflow rates inside a human airway model, and the prediction results for CHTC were reported.

The findings of this study are summarized as follows:

(1) Two types of computer models were used for analyzing CHTC in the respiratory tract, and differences of approximately 20% in average CHTC values were confirmed. The numerical errors in the two computer models were perfectly identical, so this discrepancy was caused by differences in airway geometry and reflected individual specificity. If this difference is considered, the prediction results for CHTC based on CFD using a low-Reynolds-number-type k-ε model reasonably approximate *in vitro* measured data from the literature.
(2) Comparing the results of the steady and transient simulations, time-averaged convective heat flux was reasonably consistent and the assumption of steady-state breathing for analyzing average CHTC in airway models was shown to be appropriate.
(3) The calculation obtained for average CHTC as a function of breathing airflow rate will contribute to the improvement of prediction accuracy for a thermoregulation model by improving the prediction accuracy for sensible heat transfer inside the human respiratory tract.

Acknowledgments

This project was partially supported by a Grant-in-Aid for Scientific Research (JSPS 15H04086), a Health Labour Sciences Research Grant (H27-C-009) and Postdoctoral Fellowship Program 2015 from Toshiba International Foundation.

Nomenclature

BSA	Body surface area (m^2)
CHTCs	Convective heat transfer coefficients
CT	Computed tomography
C_{res}	Rates of convective heat loss per unit area of body surface (W/m^2)
D_T	Trachea diameter (m)
k	Turbulent kinetic energy (m^2/sec^2)
Nu	Nusselt number
Pr	Prandtl number (μ C_p/k)
Q_c	Convective heat flux [W/m^2]
Re	Reynolds number
T_{air}	Air inhaled (ambient) in the airway model (K)
T_w	Constant tissue wall surface temperature (K)
u	Representative axial velocity (m/s)

Greek symbols

μ	Dynamic viscosity (kg/ms)
ρ	Fluid density (kg/m^3)
ν	Kinetic molecular viscosity (m^2/sec)
α	Thermal diffusion coefficient (m^2/sec)

References

[1] W.J. Fisk, D. Black, G. Brunner, Changing ventilation rates in U.S. offices: implications for health, work performance, energy, and associated economics, Build. Environ. 47 (2012) 368–372.
[2] W.J. Fisk, A.G. Mirer, M.J. Mendell, Quantitative relationship of sick building syndrome symptoms with ventilation rates, Indoor Air 19 (2009) 159–165.
[3] Y. Fan, K. Ito, Energy consumption analysis intended for real office space with energy recovery ventilator by integrating BES and CFD approach, Build. Environ. 52 (3) (2012) 57–67.
[4] Y. Fan, K. Ito, integrated building energy-computational fluid dynamics simulation for estimating the energy-saving effect of energy recovery ventilator with CO_2 demand-controlled ventilation system in office space, Indoor Built Environ. 23 (6) (2014) 785–803.
[5] Y. Fan, K. Kameishi, S. Onishi, K. Ito, Field-based Study on Energy saving effects of CO_2 demand controlled ventilation in office with application of energy recovery ventilators, Energ Build. 68 (2014) 412–422.
[6] Y. Fan, K. Ito, Optimization of indoor environmental quality and ventilation load in office space by multilevel coupling with BES and CFD, Int. J. Build. Simul. 7 (2014) 649–659.
[7] K. Ito, integrated numerical simulation with fungal spore deposition and subsequent fungal growth on bathroom wall surface, Indoor Built Environ. 22 (6) (2013) 881–896.
[8] N.L. Phuong, K. Ito, Investigation of flow pattern in a realistic replica model of human respiratory tract using PIV, Build. Environ. 94 (2015) 504–515.
[9] K. Ito, K. Inthavong, T. Kurabuchi, T. Ueda, T. Endo, T. Omori, H. Ono, S. Kato, K. Sakai, Y. Suwa, H. Matsumoto, H. Yoshino, W. Zhang, J. Tu, CFD benchmark tests for indoor environmental problems: part 1 isothermal/non-isothermal

flow in 2D and 3D room model, Int. J. Archit. Eng. Technol. 2 (1) (2015) 1–22, http://dx.doi.org/10.15377/2409-9821.2015.02.01.1.
[10] K. Ito, K. Inthavong, T. Kurabuchi, T. Ueda, T. Endo, T. Omori, H. Ono, S. Kato, K. Sakai, Y. Suwa, H. Matsumoto, H. Yoshino, W. Zhang, J. Tu, CFD benchmark tests for indoor environmental problems: part 2 cross-ventilation airflows and floor heating systems, Int. J. Archit. Eng. Technol. 2 (1) (2015) 23–49, http://dx.doi.org/10.15377/2409-9821.2015.02.01.2.
[11] K. Ito, K. Inthavong, T. Kurabuchi, T. Ueda, T. Endo, T. Omori, H. Ono, S. Kato, K. Sakai, Y. Suwa, H. Matsumoto, H. Yoshino, W. Zhang, J. Tu, cfd benchmark tests for indoor environmental problems: part 3 numerical thermal manikins, Int. J. Archit. Eng. Technol. 2 (1) (2015) 50–75, http://dx.doi.org/10.15377/2409-9821.2015.02.01.3.
[12] K. Ito, K. Inthavong, T. Kurabuchi, T. Ueda, T. Endo, T. Omori, H. Ono, S. Kato, K. Sakai, Y. Suwa, H. Matsumoto, H. Yoshino, W. Zhang, J. Tu, CFD benchmark tests for indoor environmental problems: part 4 air-conditioning airflows, residential kitchen airflows and fire-induced flow, Int. J. Archit. Eng. Technol. 2 (1) (2015) 76–102, http://dx.doi.org/10.15377/2409-9821.2015.02.01.4.
[13] S. Murakami, S. Kato, J. Zeng, Combined simulation of airflow, radiation and moisture transport for heat release from a human body, Build. Environ. 35 (6) (2000) 489–500.
[14] S. Murakami, Analysis and design of micro-climate around the human body with respiration by CFD, Indoor Air 14 (S7) (2004) 144–156.
[15] D.N. Sorensen, L.K. Voigt, Modeling flow and heat transfer around a seated human body by computational fluid dynamics, Build. Environ. 38 (2004) 753–762.
[16] N.P. Gao, J.L. Niu, CFD study of the thermal environment around a human body, A review, Indoor Built Environ. 14 (2005) 5–16.
[17] N.P. Gao, H. Zhang, J.L. Niu, Investigating indoor air quality and thermal comfort using a numerical thermal manikin, Indoor Built Environ. 16 (1) (2007) 7–17.
[18] J.A.J. Stolwijk, A Mathematical Model of Physiological Temperature Regulation in Man, NASA contractor report, 1971.
[19] A.P. Gagge, A.P. Fobelets, L.G. Berglund, A standard predictive index of human response to the thermal environment, ASHRAE Trans. 92 (1986) 709–731.
[20] C.E. Smith, A Transient, Three-dimensional Model of the Human Thermal System, PhD Thesis, Kansas State University, 1991.
[21] D. Fiala, K.J. Lomas, M. Stohrer, Computer prediction of human thermoregulatory and temperature responses to a wide range of environmental conditions, Int. J. Biometeorol. 45 (2001) 143–159.
[22] Y. Kobayashi, S. Tanabe, Development of JOS-2 human thermoregulation model with detailed vascular system, Build. Environ. 66 (2013) 1–10.
[23] S. Takada, T. Matsushita, Modeling of moisture evaporation from the skin, eyes and airway to evaluate sensations of dryness in low-humidity environments, J. Bldg Phys. 36 (4) (2013) 422–437.
[24] X. Li, K. Inthavong, J. Tu, Particle inhalation and deposition in a human nasal cavity from the external surrounding environment, Build. Environ. 47 (2012) 32–39.
[25] K. Inthavong, Q.J. Ge, X.D. Li, J. Tu, Detailed predictions of particle aspiration affected by respiratory inhalation and airflow, Atmos. Environ. 62 (2012) 107–117.
[26] L.M. Hanna, P. Scherer, Regional control of local airway heat and water vapor losses, J. Appl. Physiol. 61 (1986) 624–632.
[27] E.R. McFadden Jr., B.M. Pichurko, H.F. Bowman, E. Ingenito, S. Burns, N. Dowling, J. Solway, Thermal mapping of the airways in humans, J. Appl. Physiol. 58 (1985) 564–570.
[28] T. Keck, R. Leiacker, H. Riechelmann, G. Rettinger, Temperature profile in the nasal cavity, Laryngoscope 110 (2000) 651–654.
[29] P. Rouadi, F.M. Baroody, D. Abbott, E. Naureckas, J. Solway, R.M. Nacleiro, A technique to measure the ability of the human nose to warm and humidify air, J. Appl. Physiol. 87 (1999) 400–406.
[30] P. Webb, Air temperatures in respiratory tracts of resting subjects in cold, J. Appl. Physiol. 4 (1951) 378–382.
[31] D.J. Willatt, Continuous infrared thermometry of the nasal mucosa, Rhinology 31 (1993) 63–67.
[32] P. Assanasen, F.M. Baroody, E. Naureckas, R.M. Naclerio, Warming of feet elevates nasal mucosal surface temperature and reduces the early response to nasal challenge with allergen, J. Allergy Clin. Immunol. 104 (1999) 285–293.
[33] P. Cole, Air conditioning, in: P. Cole (Ed.), The Respiratory Role of the Upper Airways, Mosby Year Book, St. Louis, 1992, pp. 102–106.
[34] S. Naftali, M. Rosenfeld, M. Wolf, D. Elad, The air-conditioning capacity of the human nose, Ann. Biomed. Eng. 33 (4) (2005) 545–553.
[35] J. Lindemann, T. Keck, K. Wiesmiller, B. Sander, H.J. Brambs, G. Rettinger, D. Pless, A numerical simulation of intranasal air temperature during inspiration, Laryngoscope 114 (2004) 1037–1041.
[36] G. Mlynski, S. Grutzenmacher, S. Plontke, B. Mlynski, C. Lang, Correlation of nasal morphology and respiratory function, Rhinology 39 (2001) 197–201.
[37] E. Marchandise, M. Willemet, V. Lacroix, A numerical hemodynamic tool for predictive vascular surgery, Med. Eng. Phys. 31 (2009) 131–144.
[38] T. Keck, J. Lindemann, Simulation and air-conditioning in the nose, Laryngo Rhino Otol. 89 (Suppl. 1) (2010) S1–S14.
[39] J. Lindemann, T. Keck, K. Wiesmiller, B. Sander, H.J. Brambs, G. Rettinger, et al., A numerical simulation of intranasal air temperature during inspiration, Laryngoscope 114 (2004) 1037–1041.
[40] D. Pless, T. Keck, K. Wiesmiller, G. Rettinger, A.J. Aschoff, T.R. Fleiter, J. Lindemann, Numerical simulation of air temperature and airflow patterns in the human nose during expiration, Clin. Otolaryngol. Allied Sci. 29 (2004) 642–647.
[41] C.B. Frederick, M.L. Bush, L.G. Lomax, K.A. Black, L. Finch, J.S. Kimbell, K.T. Morgan, R.P. Subramaniam, J.B. Morris, J.S. Ultman, Application of a hybrid computational fluid dynamics and physiologically based inhalation model for interspecies dosimetry, extrapolation of acidic vapors in the upper airways, Toxicol. Appl. Pharmacol. 152 (1998) 211–231.
[42] F.Y. Boisa, M. Jameic, H.J. Clewelld, PBPK modelling of inter-individual variability in the pharmacokinetics of environmental chemicals, Toxicology 278 (2010) 256–267.
[43] M.E. Andersen, T. Green, C.B. Frederick, M.S. Bogdanffy, Physiologically based pharmacokinetic (PBPK) models for nasal tissue dosimetry of organic esters: Assessing the state-of-knowledge and risk assessment applications with methyl methacrylate and vinyl acetate, Regul. Toxicol. Pharmacol. 36 (2002) 234–245.
[44] R.A. Corley, S. Kabilan, A.P. Kuprat, J.P. Carson, R.E. Jacob, K.R. Minard, J.G. Teeguarden, C. Timchalk, S. Pipavath, R. Glenny, D.R. Einstein, Comparative risks of aldehyde constituents in cigarette smoke using transient computational fluid dynamics/physiologically based pharmacokinetic models of the rat and human respiratory tracts, Toxicol. Sci. (2015) 1–24.
[45] D. Wu, S. Miyawaki, M.H. Tawhai, E.A. Hoffman, C.L. Lin, A Numerical Study of Water Loss Rate Distributions in MDCT-based Human Airway Models Annals of Biomedical Engineering, vol. 43, No. 11, 2015, pp. 2708–2721.
[46] ANSYS, Inc. ANSYS Fluent 14.5 User's Guide; 2012.
[47] D.N. Sorensen, P.V. Nielsen, Quality control of computational fluid dynamics in indoor environments, Indoor Air 13 (2003) 2–17.
[48] K. Abe, T. Kondoh, Y. Nagano, A new turbulence model for predicting fluid flow and heat transfer in separating and reattaching flows-I. Flow field calculations, Int. J. Heat. Mass Transf. 37 (1) (1994) 139–151.
[49] K. Abe, T. Kondoh, Y. Nagano, A new turbulence model for predicting fluid flow and heat transfer in separating and reattaching flows-II. Thermal field calculations, Int. J. Heat. Mass Transf. 38 (8) (1995) 1467–1481.
[50] V. Pantakar, Numerical Heat Transfer and Fluid Flow, McGraw-Hill, New York, 1980.
[51] K.W. Stapleton, E. Guentsch, M.K. Hoskinson, W.H. Finlay, On the suitability of k-epsilon turbulence modeling for aerosol deposition in the mouth and throat: a comparison with experiment, J. Aerosol Sci. 31 (2000) 739–749.
[52] J.K. Gupta, C.-H. Lin, Q. Chen, Characterizing exhaled airflow from breathing and talking, Indoor Air 20 (2009) 31–39.
[53] J.K. Gupta, C.-H. Lin, Q. Chen, Flow dynamics and characterization of a cough, Indoor Air 19 (2009) 517–525.
[54] Y. Kadota, T. Matsuo, S.J. Yoo, N.L. Phuong, K. Ito, Development of computer simulated person with numerical airway model, part 3 breathing air quality prediction by improved unsteady breathing flow model, Indoor Air (2014). Hong Kong, July 7–12, 2014, Paper ID: HP0732.
[55] T. Keck, R. Leiacker, A. Heinrich, S. Kuhneman, G. Rettinger, Humidity and temperature profile in the nasal cavity, Rhinotegy 38 (2000) 167–171.
[56] P.O. Fanger, Thermal comfort: Analysis and Applications in Environmental Engineering, Danis 2014, h Technical Press, 1970.
[57] M.L. Nuckols, J.L. Zumrick, C.E. Johnson, Heat and water vapor transport in the human upper airways at hyperbaric conditions, J. Biomech. Eng. 105 (1983) 24–30.
[58] W. Cai, N. Su, X. Liu, Unsteady convection flow and heat transfer over a vertical stretching surface, Plos One 9 (9) (2014) e107229.
[59] D. Gupta, L. Kumar, B. Singh, Finite element solution of unsteady mixed convection flow of micropolar fluid over a porous shrinking sheet, Sci. World J. 2014 (2014). Article ID 362351, http://dx.doi.org/10.1155/2014/362351.

Survey Report
[*Journal of Environmental Chemistry* Vol.25, No.4, pp.207-214, 2015]

Survey of Isothiazolinones and Other Preservatives in Household Wet Tissue Products in Japan

Tsuyoshi KAWAKAMI, Kazuo ISAMA and Yoshiaki IKARASHI

Division of Environmental Chemistry, National Institute of Health Sciences
(1-18-1 Kamiyoga, Setagaya, Tokyo 158-8501, Japan)

[Received January 29, 2015; Accepted August 10, 2015]

Summary

Recently, many cases of contact dermatitis due to isothiazolinone preservatives in several types of household products used for cooling the body have been reported. As a result, the concentrations of isothiazolinone preservatives in these products were investigated. However, concentrations of isothiazolinone preservatives in other types of household products have not been studied adequately. In this study, 19 preservatives (including isothiazolinones) in 32 wet tissue products were investigated because these products come in direct contact with the skin. 2-Methyl-4-isothiazolin-3-one (MI), 5-chloro-2-methyl-4-isothiazolin-3-one (CMI), and benzisothiazolin-3-one (BIT) were detected in 19 samples (0.46-48 μg/g-wet), 17 samples (trace amount [tr.]-52 μg/g-wet), and one sample (67 μg/g-wet), respectively. Five types of parabens were detected in 21 samples (tr.-834 μg/g-wet). 2-Bromo-2-nitropropane-1,3-diol (Bronopol), 3-iodo-2-propynyl *N*-butylcarbamate (IPBC), and phenoxyethanol were detected in 12 samples (4.7-254 μg/g-wet), 11 samples (tr.-62 μg/g-wet), and 4 samples (65-1159 μg/g-wet), respectively. The concentration levels of isothiazolinone preservatives detected in this study perhaps induce allergic contact dermatitis in patients who are already sensitive to these preservatives. However, only 3 products described the use of isothiazolinone preservatives and a cautionary note about the possibility of contact dermatitis due to isothiazolinone preservatives was not provided. We also found that preservatives detected in the samples were different from those indicated on the product (in some cases, name of preservatives were not indicated at all). The use of such products may expose consumers to the risk of contact dermatitis; moreover, when contact dermatitis occurs, the identification of the substance that causes it may be delayed. Therefore, it is desirable that manufacturers provide information about the components of wet tissue products on the product labels.

Key words: wet tissue, preservative, isothiazolinone, contact dermatitis, household product

Introduction

Recently, several types of household products used for cooling the body, such as gel-products (containing superabsorbent polymers) and polyvinyl alcohol (PVA) towels, have been developed, and the sale of these products in Japan has increased[1, 2]. However, several cases of contact dermatitis due to such products containing isothiazolinone preservatives have been reported[3, 4]. As a result, a voluntary recall of gel-products was issued by the supplier[5] and information about the use of PVA cooling towel was provided by the National Consumer Affair Center of Japan[4]. Therefore, we have studied the concentration levels of several isothiazolinone preservatives in gel-products[6] and PVA cooling towels[7, 8].

Additionally, many cases of contact dermatitis related to isothiazolinone preservatives in various kinds of household products, such as paints, fabric softeners, detergent for toilet, ironing water, and wet tissue (wet wipe) products, have been reported in Europe and the U.S.A.[9]. It is necessary to grasp the actual concentration levels of isothiazolinone preservatives in these products. However, only a few studies have been conducted on isothiazolinone preservatives in household products, such as our previous studies on cooling products[6-8] and household non-formalin adhesives for wallpaper[10] in Japan. Thus, to prevent the occurrence of allergic contact dermatitis, a survey of isothiazolinone preservatives in household products to which consumers can be exposed is necessary.

Many cases of contact dermatitis due to isothiazolinone preservatives in wet tissue products have been reported in Europe and the USA[9,11-19] because wet tissue products come in direct contact with the skin. Thus, we investigated the concentrations of five isothiazolinone preservatives in wet tissue products. Furthermore, non-isothiazolinone preservatives in wet tissue products, such as 2-bromo-2-(bromomethyl)pentanedinitrile (methyldibromo glutaronitrile (MDBGN)) and 3-iodo-2-propynyl *N*-butylcarbamate (IPBC), have been reported to cause contact dermatitis[15,20]. Therefore, 14 types of non-isothiazolinone preservatives in wet tissue products were also investigated in this study.

Materials and methods

Samples

Since the consumer can easily purchase wet tissue products, 32 wet tissue products samples were purchased from several 100-yen

stores in Japan from January to February 2014 (details of these samples are provided in Table 1). Wet tissue products for infants were not purchased, because they are classified as cosmetic products in Japan.

Materials

2-Methyl-4-isothiazolin-3-one (MI) and 5-chloro-2-methyl-4-isothiazolin-3-one (CMI) were purchased from Waterstone Technology, LLC as a mixture (MI: 3.63%, CMI: 10.85%). Benzoisothiazolin-3-one (BIT), 2-*n*-octyl-4-isothiazolin-3-one (OIT), parabens (PBs) [methylparaben (Me-PB), ethylparaben (Et-PB), propylparaben (Pr-PB), isopropylparaben (Isopro-PB), butylparaben (Bu-PB), isobutylparaben (Isobu-PB), and benzylparaben (Be-PB)], benzoic acid (BA), phenoxyethanol (PE), 2-bromo-2-nitropropane-1,3-diol (Bronopol: BP), 5-bromo-5-nitro-1,3-dioxane (Bronidox), 2-mercaptobenzothiazole (MBT), and 3-iodo-2-propynyl *N*-butylcarbamate (IPBC) were obtained from Tokyo Kasei Kogyo Co., Ltd. 4,5-Dichloro-2-*n*-octyl-4-isothiazolin-3-one (2Cl-OIT) and 2-bromo-2-(bromomethyl)-pentanedinitrile (methyldibromo glutaronitrile: MDBGN) were purchased from AK Scientific Inc. and Sigma-Aldrich, respectively. Their abbreviation, CAS number, chemical formula, and molecular weight are listed in Table 2.

HPLC grade of acetonitrile and pesticide residue analysis grade of methanol were purchased from Sigma-Aldrich. Liquid chromatography/mass spectrometry grade of formic acid was obtained from Wako Pure Chemical Industries, Ltd. Milli-Q water was produced using a Milli-Q Synthesis A10 system (Merck Millipore, Tokyo, Japan).

Sample processing

In the first step, several sheets of wet tissue products were taken out from the upper part of the package. Then, these sheets were cut into small pieces and 1.0 g of the sample was weighed. This weighted sample was placed into a glass tube with 20 mL of methanol and shaken for 30 min using a horizontal shaker. After shaking, the sample was filtered using a suction funnel with a glass filter. The residue was washed with methanol and the wash was combined with the filtrate. The sample solution was concentrated to less than 5 mL with a rotary evaporator while the temperature of the water bath was maintained below 40℃. The volume of the sample solution was subsequently adjusted to 5 mL using methanol. The sample solution was filtered using a PTFE filter (pore size: 0.20 μm, ADVANTEC) and analyzed by high performance liquid chromatography with a photo diode array detector (HPLC/PDA).

HPLC/PDA analysis

All samples were analyzed using a Shimadzu NexeraX2 HPLC

Table 1 List of wet tissue samples studied

No.	Country of manufacture	The ingredients described on the product[a]
1	Japan	ethanol, bactericide, benzalkonium chloride
2	Japan	water, propylene glycol, cetylpyridinium chloride, ethyl benzoate, methyl benzoate, aloe extract
3	China	water, ethanol, PG, benzalkonium chloride, methylparaben, ethylparaben
4	Japan	water, PG, methylparaben, ethylparaben, benzalkonium chloride
5	Japan	water, benzalkonium chloride, BG, iodopropynyl butylcarbamate, grapefruit seed extract, sodium hydrogen carbonate
6	Japan	water, propylene glycol, cetylpyridinium chloride, ethylparaben, methylparaben, silver ion water
7	Japan	water, ethanol, PG, methylparaben, ethylparaben, benzalkonium chloride
8	Japan	ethanol, bactericide, benzalkonium chloride
9	Japan	ethanol, paraben, cation, PG, purified water
10	Japan	ethanol, benzalkonium chloride, paraben, purified water, perfume
11	Japan	propyl parahydroxybenzoate, chlorhexidine gluconate, ethanol, perfume, purified water
12	South Korea	water, ethanol, propylene glycol, chlorobenzal, methylchloroisothiazolinone, methylisothiazolinone, polyaminopropyl biguanide, green tea extract
13	Japan	water, PG, benzalkonium chloride, iodopropynyl butylcarbamate
14	Japan	water, BG, benzalkonium chloride, iodopropynyl butylcarbamate, tea extract
15	Japan	water, propylene glycol, methylparaben, organic compound containing nitrogen and sulfur, ethylparaben, propylparaben, silver ion
16	China	purified water, ether, bactericide
17	China	water, PG, methylparaben, ethylparaben, propylparaben, propylene glycol, paraben, benzalkonium chloride
18	Japan	water, BG, benzalkonium chloride, iodopropynyl butylcarbamate
19	Japan	water, ethanol, BG, benzalkonium chloride, iodopropynyl butylcarbamate
20	Japan	water, PG, methylparaben, ethylparaben, propylparaben, benzalkonium chloride
21	Japan	water, propylene glycol, ethyl parahydoxybenzoate, methyl parahydoroxybenzoate, benzalkonium chloride
22	China	water, propylene glycol, aloe vera, cocamidopropyl betaine, vitamin E, citric acid, methylparaben, bronopol, ethylenediaminetetraacetic acid, methylisothiazoline
23	China	water, ethanol, paraben, benzalkonium chloride
24	Japan	water, PG, methylparaben, ethylparaben、propylparaben, benzalkonium chloride
25	Japan	water, propylene glycol, methylparaben, ethylparaben, benzalkonium chloride
26	Japan	purified water, propylene glycol, pehnoxyethanol, paraben, benzethonium chloride, glycerine, cetylpyridinium chloride, aloe extract, perfume
27	China	water, PG, methylparaben, ethylparaben, propylparaben, tea extract, benzalkonium chloride
28	China	purified water, paraben, benzalkonium chloride
29	China	water, propylene glycol, benzalkonium chloride, aloe vera, vitamin E, citric acid, methylisothiazolin, methylparabene, bronopol, ethylenediaminetetraacetic acid
30	China	purified water, ethanol, benzalkonium chloride
31	Japan	ethanol, purified water, benzalkonium chloride, paraben, BG
32	Japan	water, ethanol, bactericide, preservative

[a] List of ingredients provided on the product label.

system (Shimadzu, Kyoto, Japan) consisting of two LC-30AD pumps, a CTO-30A column oven, an SPD-M30A photodiode array detector, an SIL-30AC auto sampler, and a CBM-20A communication bus module. System control and data calibration were carried out using the Lab Solutions software (ver. 6. 11.) (Shimadzu, Kyoto, Japan). An InertSustain® Phenyl column (length 150 mm, internal diameter 3.0 mm, particle size 3 μm; GL Sciences, Inc., Tokyo, Japan) was used for separating the target compounds. Eluent A of ultrapure water containing 0.1% formic acid and eluent B of acetonitrile were used as the mobile phase. The gradient elution began with 25% of eluent B, which was held constant for 2 min, and increased linearly to 30% over 9 min, which was held constant for another 3 min. Then, eluent B increased linearly to 90% over 6 min, which was held constant for another 5.5 min. These gradient conditions are similar to those in the previous study[7] with minor modifications. The flow rate, injection volume, and oven temperature were 0.6 mL/min, 5 μL, and 40℃ , respectively. The monitoring wavelength ranged from 190 to 600 nm and UV-Vis spectra of the preservatives measured by PDA were used for identification of target compounds. The wavelengths used for the quantification of the analytes are shown in Table 3.

Results and discussion

Limits of detection and quantification

The HPLC chromatogram of the standard solution is shown in Fig. 1. Good separation of all the preservatives was observed. The retention times of the compound are listed in Table 3. The relative standard deviation of the retention times of every compound was below 0.06% (n=5).

Recovery tests were conducted by adding every compound to the sample (No.5) that did not contain the target compounds, except for IPBC that was detected below the limit of quantification (LOQ). The added amounts of the compounds were as follows: MI: 1.68 μg/g-wet; Bronidox, MDBGN, and IPBC: 50 μg/g-wet; other analytes: 5.0 μg/g-wet. The recovery tests were conducted in quardruplicate. The recoveries of target compounds and their coefficients of variation were 71–109% and 1.2–5.5%, respectively (Table 3). The limit of detection (LOD) was calculated according to JIS K 0124:2011[21] using the standard deviation (SD) and t-value (t=4.71 for n=4) obtained from the recovery tests. LOQ was calculated as ten times of SD[22]. The LODs and LOQs are listed in Table 3. The LODs and LOQs of the analytes were in the ranges of 0.12–5.6 μg/g and 0.25–12 μg/g, respectively. The LODs and LOQs of bronidox, MDBGN, and IPBC were higher than those of other compounds because of their lower sensitivity than other chemicals.

Concentrations of the target compounds in wet tissue samples

The concentrations of the target compounds in the wet tissue samples are listed in Table 4. Three types of isothiazolinones (MI, CMI, and BIT), five types of parabens (Me-PB, Et-PB, Pro-PB, Isobu-PB, and Bu-PB), BP, PE, and IPBC were detected in the samples. Other preservatives were not detected. A representative HPLC chromatogram obtained from sample No.6 is shown in Fig. 2. MI and CMI were detected in 19 samples (0.46–48 μg/g-wet) and 17 samples (trace amount [tr.]-52 μg/g-wet), respectively. BIT was detected in one sample (67 μg/g-wet). The detection frequencies of PBs were in the following order: Me-PB (21 samples, tr.-834 μg/g-wet), Et-PB (20 samples, tr.-748 μg/g-wet), Pro-PB (6 samples, 30–328 μg/g-wet), Isobu-PB (one sample, 42 μg/g-wet), and Bu-PB (one sample, 73 μg/g-wet). BP, IPBC, and PE were detected in 12 samples (4.7–254 μg/g-wet), 11 samples (tr.-62 μg/g-wet), and 4 samples (65–1159 μg/g-wet), respectively.

Table 2 Abbreviation, CAS number, chemical formula, and molecular weight of preservatives investigated

		Abbreviation	CAS number	Chemical formula	Molecular weight
Isothiazolinones	2-Methyl-4-isothiazilin-3-one	MI	2682-20-4	C_4H_5NOS	115.15
	5-Choro-2-methyl-4-isothiazolin-3-one	CMI	26172-55-4	C_4H_4ClNOS	149.60
	Benzisothiazolin-3-one	BIT	2634-33-5	C_7H_5NOS	151.19
	2-n-Octyl-4-isothiazolin-3-one	OIT	26530-20-1	$C_{11}H_{19}NOS$	213.30
	4,5-Dichloro-n-octyl-4-isothiazolin-3-one	2Cl-OIT	64359-81-5	$C_{11}H_{17}Cl_2NOS$	282.20
Parabens	Methyl 4-hydroxybenzoate (methylparaben)	Me-PB	99-76-3	$C_8H_8O_3$	152.15
	Ethyl 4-hydroxybenzoate (ethylparaben)	Et-PB	120-47-8	$C_9H_{10}O_3$	166.18
	Isopropyl 4-hydroxybenzoate (isopropylparaben)	Isopro-PB	4191-73-5	$C_{10}H_{12}O_3$	180.20
	Propyl 4-hydroxybenzoate (propylparaben)	Pro-PB	94-13-3	$C_{10}H_{12}O_3$	180.20
	Isobutyl 4-hydroxybenzoate (isobutylparaben)	Isobu-PB	4247-02-3	$C_{11}H_{14}O_3$	194.23
	Butyl 4-hydroxybenzoate (butylparaben)	Bu-PB	94-26-8	$C_{11}H_{14}O_3$	194.23
	Benzyl 4-hydroxybenzoate (benzylparaben)	Be-PB	94-18-8	$C_{14}H_{12}O_3$	228.25
Others	2-Bromo-2-nitropropane-1,3-diol (bronopol)	BP	52-51-7	$C_3H_6BrNO_4$	199.99
	2-Phenoxyethanol	PE	122-99-6	$C_8H_{10}O_2$	138.16
	Benzoic acid	BA	65-85-0	$C_7H_6O_2$	122.12
	5-Bromo-5-nitro-1,3-dioxane	Bronidox	30007-47-7	$C_4H_6BrNO_4$	212.00
	2-Mercaptobenzothiazole	MBT	149-30-4	$C_7H_5NS_2$	167.24
	2-Bromo-2-(bromomethyl)-pentanedinitrile (methyldibromo glutaronitrile)	MDBGN	35691-65-7	$C_6H_6Br_2N_2$	265.93
	3-Iodo-2-propynyl N-butylcarbamate	IPBC	55406-53-6	$C_8H_{12}INO_2$	281.09

Table 3 Retention time, quantifying wavelength, limit of detection (LOD), limit of quantification (LOQ), and recovery of target compounds

Chemicals[a]	Retention time (min)	Wavelength (nm)	LOD[b] (μg/g-wet)	LOQ[c] (μg/g-wet)	Recovery[b] (%)	C.V.[d] (%)
MI	1.73	273	0.12	0.25	106	1.5
BP	2.17	195	0.40	0.84	95	1.8
CMI	2.72	273	1.1	2.3	96	4.8
BIT	3.29	226	0.72	1.5	104	3.0
PE	4.22	195	1.0	2.2	94	4.6
BA	4.52	195	0.14	0.30	106	1.3
Me-PB	4.93	256	0.35	0.75	108	2.3
Bronidox	6.33	195	5.6	12	81	2.9
Et-PB	7.37	256	0.41	0.87	108	3.0
MBT	8.27	322	0.91	1.9	71	5.5
MDBGN	8.67	195	4.5	10	92	2.6
Isopro-PB	10.37	256	0.45	0.95	107	1.8
Pro-PB	11.02	256	0.61	1.3	107	2.4
Isobu-PB	15.16	256	0.36	0.76	109	1.4
Bu-PB	15.88	256	0.30	0.64	109	1.2
IPBC	17.00	195	2.8	5.9	89	1.3
OIT	17.46	273	0.64	1.4	107	2.5
Be-PB	17.68	256	0.73	1.6	105	3.0
2Cl-OIT	19.80	283	0.93	2.0	80	5.0

[a] The definition of abbreviations are described in Table 2.

[b] LOD was calculated according to JIS K0124:2011 using the standard deviation (SD) and t-value (t = 4.71 for n = 4) obtained from the recovery test. (MI: 1.67 μg/g-wet; Bronidox, MDBGN, and IPBC: 50 μg/g-wet; others: 5 μg/g-wet)

[c] LOQ was calculated as ten times of SD.

[d] Coefficient of variation.

Although the use of MI and CMI was indicated on three samples (No.12, No.22, and No.29), we found that both MI and CMI were present in many other samples. The concentrations of MI and CMI in most of the wet tissue samples were lower than those in PVA towels[8, 9]. It is possible that MI and CMI, which were also detected in wet tissue samples in which the presence of isothiazolinones was not indicated, might be intentionally used as preservatives because of their minimum inhibitory concentrations (MICs) for fungi and bacteria, which are 2–9 ppm (as mixture of MI and CMI) and 0.75–9 ppm (as mixture of MI and CMI) [23], respectively. However, it is also possible that MI and CMI were contaminated during manufacturing because several types of other preservatives were detected in the same sample. Although BIT was not detected in the gel-products used for cooling, PVA towels[7-9], and adhesives for wall-paper[10], it was detected in the wet tissue sample (No.15) in this study. For this product, the use of "organic compound contained nitrogen and sulfur" was indicated on the product label; this compound may correspond to BIT. The concentration of BIT detected from No.15 was higher than its MIC (5–49 ppm for fungi and bacteria)[24]. PBs were detected in many samples; some PBs detected in the sample did not coincide with the descriptions provided with the products. Although the use of BP was indicated for two products (No.22 and 29), we also detected BP in other samples. BP was detected in the samples together with MI and CMI. A similar tendency was observed in PVA cooling towels[9]. Since a mixture of BP, MI, and CMI is used as a water-treatment agent in various industrial processes[25], the mixture may also be used for wet tissue products.

Safety of wet tissue products

In December 2014, Cosmetics Europe - The Personal Care Association recommended that the use of MI in leave-on skin products (including cosmetic wet wipes) be discontinued because of an increase in the number of patients showing a positive reaction to MI[26]. The wet tissue products investigated in this study are not cosmetic products, and hence, they fall under this recommendation. The concentrations of the mixture of MI and CMI (in μg/g-wet) observed in two samples (No.6 and 28) were higher than the regulated values (as a mixture: 15 μg/g, MI: 3.75 μg/g, CMI: 11.25 μg/g) for cosmetic products in the EU[27], the USA[28], and Japan[29]. Furthermore, cases of contact dermatitis caused by wet tissue products containing MI or the mixtures of MI and CMI (10–34 μg/g) have been reported in previous studies[11, 13, 19]. Therefore, it is necessary to use wet tissue products with care, especially for patients who are already sensitive to isothiazolinone preservatives, because wet tissue products come in direct contact with the skin. Furthermore, since some cases of perianal allergic contact dermatitis due to the use of wet tissues containing MI and CMI around the anus have been reported[11, 12, 14, 15], these wet tissues should be used carefully in sensitive areas such as the perianal area.

In the EU, the concentration of BP in the cosmetic products is regulated to be below 0.1%[27]. Case of occupational contact dermatitis due to BP[30] and positive reactions to BP in patch tests have been reported[31, 32]. These papers reported that skin irritation and allergic responses in the patch test were induced at BP concentrations of 0.5% and 0.25%, respectively[30-32]. Since the highest concentration of BP detected in this study was 254 μg/g-wet, skin sensitization by BP in the

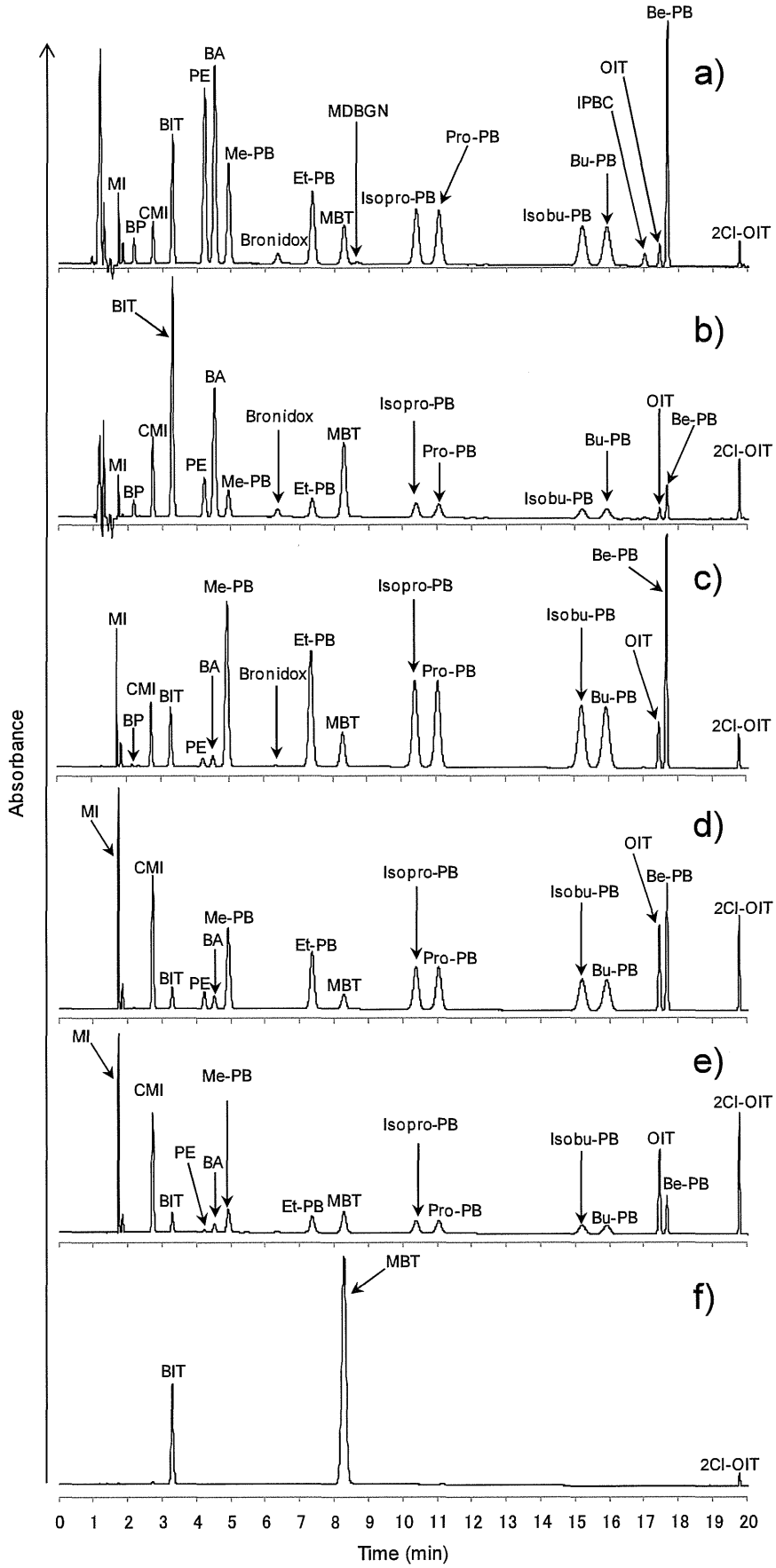

Fig. 1 HPLC chromatograms of the standard solution (MI: 6.73 μg/mL; other preservatives: 20 μg/mL). (a: 195 nm, b: 226 nm, c: 256 nm, d: 273 nm, e: 283 nm, f: 322 nm) (The definition of abbreviations are described in Table 2)

Table 4 Concentrations of preservatives in the wet tissue samples[a]

No.	Isothiazolinones (μg/g-wet)			Parabens (μg/g-wet)					Other preservatives (μg/g-wet)		
	MI	CMI	BIT	Me-PB	Et-PB	Pro-PB	Isobu-PB	Bu-PB	BP	PE	IPBC
1	-[b]	-	-	723	748	-	-	-	-	-	-
2	3.0	-	-	58	66	-	-	-	-	-	-
3	0.62	0.87	-	317	357	-	-	-	25	-	-
4	0.54	2.6	-	-	-	-	-	-	-	-	6.5
5	-	-	-	-	-	-	-	-	-	-	tr.[c]
6	8.6	19	-	103	122	-	-	-	120	-	-
7	3.7	11	-	366	176	-	-	-	46	-	-
8	-	-	-	695	729	-	-	-	-	-	-
9	1.3	5.6	-	207	100	-	-	-	5.0	-	-
10	0.80	4.6	-	382	186	-	-	-	4.7	-	-
11	-	-	-	507	-	198	-	-	-	-	-
12	3.6	7.5	-	-	-	-	-	-	-	-	-
13	0.46	3.8	-	-	-	-	-	-	6.4	-	16
14	-	-	-	-	-	-	-	-	-	-	7.8
15	-	-	67	389	206	70	-	-	-	-	-
16	2.2	tr.	-	-	-	-	-	-	-	209	27
17	-	-	-	278	147	161	-	-	-	82	19
18	-	-	-	-	-	-	-	-	-	-	6.2
19	-	-	-	-	-	-	-	-	-	-	20
20	-	-	-	834	310	328	-	-	-	-	-
21	5.0	6.5	-	57	65	-	-	-	33	-	-
22	1.1	3.1	-	tr.	tr.	-	-	-	245	-	62
23	-	-	-	615	640	-	-	-	-	-	-
24	3.7	10	-	426	199	-	-	-	33	-	-
25	3.3	9.0	-	381	192	-	-	-	28	-	-
26	-	-	-	159	54	30	42	73	-	1159	-
27	-	-	-	219	118	136	-	-	-	65	-
28	48	52	-	-	-	-	-	-	-	-	-
29	1.1	tr.	-	-	-	-	-	-	254	-	42
30	3.3	6.2	-	783	3.3	-	-	-	-	-	-
31	1.1	4.9	-	262	135	-	-	-	6.7	-	-
32	26	-	-	-	-	-	-	-	-	-	48

[a] The definition of abbreviations are described in Table 2. [b] Not detected. [c] Between the LOD and LOQ.

wet tissue products studied in this survey is not likely to occur.

Regulated values of IPBC in leave-off products, leave-on products, and deodorant products are below 0.02%, 0.01%, and 0.0075%, respectively, in the EU[27]. In Japan, the concentration of IPBC in cosmetic products must be less than 0.02%[29]. Although the use of 0.2% IPBC solution was recommended for the patch test[33], a positive reaction to 0.1% IPBC solution was reported for a patient who worked in a wood widow frame manufactory[34]. However, IPBC concentrations in wet tissue products have not been reported in the cases of contact dermatitis due to wet tissue products[15, 21]. Furthermore, the concentrations of IPBC detected in this study were lower than the regulated value in the EU. Thus, skin sensitization due to IPBC in wet tissue products studied in this survey probably did not occur. However, because IPBC was also used as a wood preservative[34] and a household antimicrobial agent[35], it is necessary to carefully use wet tissues containing IPBC for patients who are already sensitive to IPBC. Cross-reactivity between IPBC and thiurams has also been reported[33, 36] because both compounds contain carbamate functionalities. Therefore, it is necessary that patients who are already sensitized to thiurams should be careful while handling household products containing IPBC.

In Japan, the concentrations of PBs and PE used in cosmetic products and quasi-drugs must be less than 1.0%[29, 37]. The concentrations of PBs detected in this study were higher than the concentrations of other preservatives; however, the PB concentrations were below 1.0% in all samples. Furthermore, a negative patch test reaction was reported in the patch test using 0.1% PE[38]. Thus, skin sensitiza-

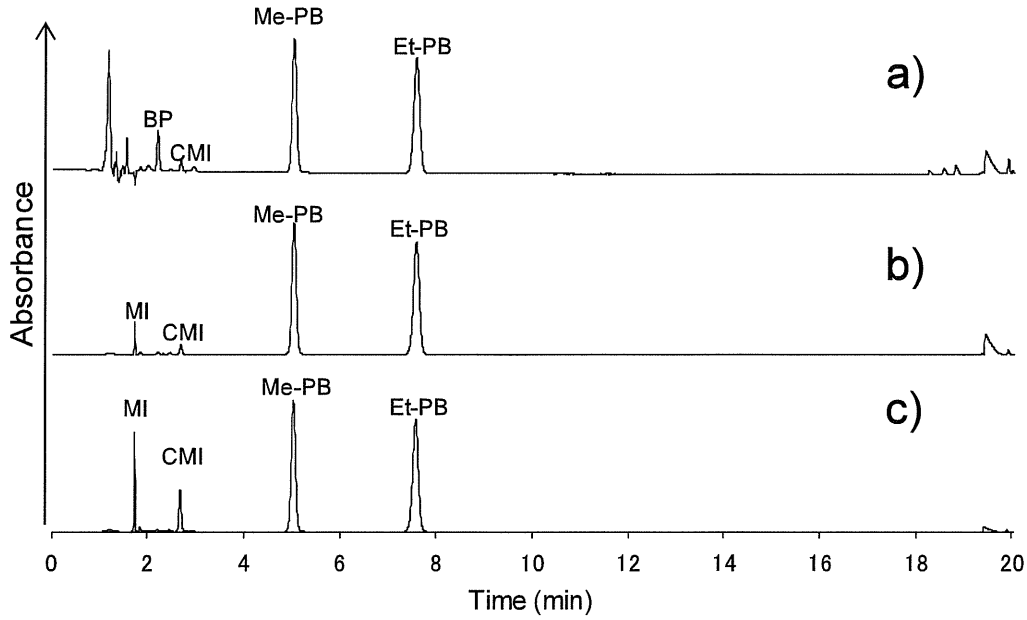

Fig. 2 HPLC chromatograms of sample solution (No.6). (a: 195 nm, b: 256 nm, c: 273 nm)
(The definition of abbreviations are described in Table 2)

tion by PBs and PE is not likely to occur in wet tissue products investigated in this survey.

Although isothiazolinone preservatives were detected in 20 products in this study, only three products indicated the use of isothiazolinone preservatives, and a cautionary note informing about the possibility of contact dermatitis due to isothiazolinone was not provided. We also found that preservatives detected in the samples were different from those indicated on the products (in some instances, name of preservatives were not indicated at all). The use of these products may expose consumers to the risk of contact dermatitis. Furthermore, it is likely that in such a situation, the identification of the substance causing contact dermatitis may be delayed when contact dermatitis due to these products occurs. Thus, it is desirable that manufacturers provide information about the components of wet tissue products on product labels.

References

1) Bank of Japan Fukuoka Branch: The effect of heat wave on personal consumption at this place, http://www3.boj.or.jp/fukuoka/topics/topics2508.pdf
2) Syukan Syogyo Publishing Co., Ltd: DAILY COSMETICS NEWS, http://www.syogyo.jp/news/2012/05/post_003709.php
3) Fukunaga, A., Nishiyama, S., Shimizu, H., Nagai, H., Horikawa, T., Mori, A., Inoue, N., Sasaki, K. and Nishigori, C.: Non-occupational allergic contact dermatitis from 2-*n*-ocytyl-4-isothiazolin-3-one in a Japanese mattress gel-sheet used for cooling. *Contact Dermatitis*, **62**, 317–318 (2010)
4) National Consumer Affair Center of Japan.: Product test - The towel used for cooling (in Japanese), http://www.kokusen.go.jp/pdf/n-20120119_1.pdf (in Japanese)
5) Office of Chemical Safety, Evaluation and Licensing Division, Pharmaceutical and Food Safety Bureau, Ministry of Health, Labour and Welfare (MHLW): http://www.nihs.go.jp/mhlw/chemical/ katei/topics/ 100324-1.pdf (in Japanese)
6) Kawakami, T., Isama, K. and Nishimura, T.: Analysis of isothiazolinones and other preservatives in gel-products used for cooling in Japan. *J. Environ. Chem.*, **22**, 205–211 (2012)
7) Kawakami, T., Isama, K. and Ikarashi, Y.: Analysis of isothiazolinone preservatives in polyvinyl alcohol cooling towels used in Japan. *J. Environ. Sci. Health A*, **49**, 1209–1217 (2014)
8) Kawakami, T., Isama, K. and Ikarashi, Y.: Analysis of 19 preservatives in polyvinyl alcohol cooling towels used in Japan by high performance liquid chromatography with photo diode array detector. *J. Environ. Anal. Chem.*, **2**, 122, Doi:10.4172/JREAC.1000122 (2015)
9) Kawakami, T., Isama, K. and Ikarashi, Y.: Contact dermatitis caused by isothiazolinone preservatives - Focusing on cases of contact dermatitis from household products. *J. Environ. Dermatol. Cutan. Allergol.*, **8**, 147–161 (2014) (in Japanese with English summary)
10) Nakashima, H., Matsunaga, I., Miyano, N. and Kitagawa, M.: Determination of antimicrobial agents in non-formalin adhesives for wallpaper. *J. Health Sci.*, **46**, 447–454 (2000)
11) Minet, A., Eggers, S., Willocx, D., Bourlond, A. and Lachapelle, J.M.: Allergic contact dermatitis from Kathon CG™ in moist toilet paper. *Contact Dermatitis*, **21**, 107–108 (1989)
12) de Groot, A.C., Baar, T.J.M., Terpstra, H. and Weyland, J.W.: Contact allergy to moist toilet paper. *Contact Dermatitis*, **24**, 135–136 (1991)
13) Guimaraens, D., Condé-Salazar, L. and Gonzalez, M.A.: Allergic contact dermatitis on the hands from chloromethylisothiazolinone in moist toilet paper. *Contact Dermatitis*, **35**, 254 (1996)
14) de Groot, A.C.: Vesicular dermatitis of the hands secondary to perianal allergic contact dermatitis caused by preservatives in moistened toilet tissues. *Contact Dermatitis*, **36**, 173–174 (1997)
15) Fields, K.S., Nelson, T. and Powell, D.: Contact dermatitis caused by baby wipe. *J. Am. Acad. Dermatol.*, **54**, S230-S232 (2006)
16) Timmermans, A., De Hertog, S., Gladys, K., Vanacker, H. and